EMISSION-LINE STARS

Kam-Ching Leung
University of Nebraska

Reference text

The Astrophysics of Emission-Line Stars

Tomokazu Kogure
Kam-Ching Leung
Springer 2007

Book Cover

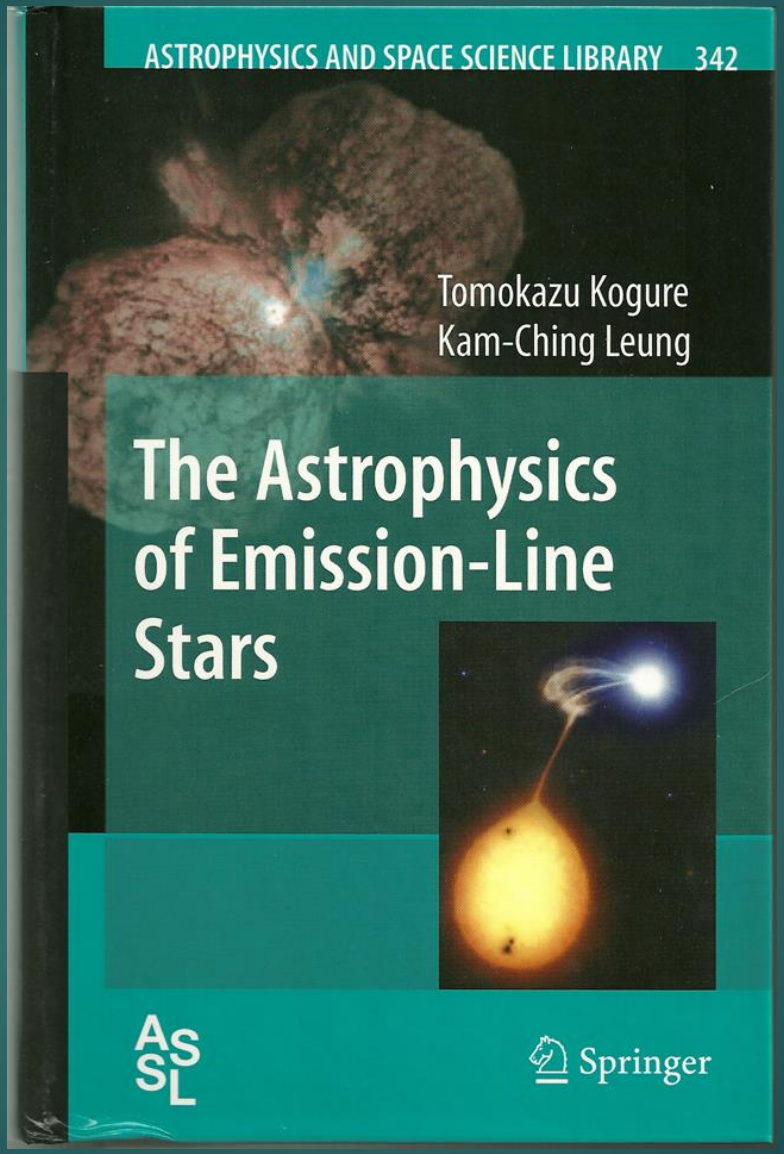
ASTROPHYSICS AND SPACE SCIENCE LIBRARY 342
Tomokazu Kogure
Kam-Ching Leung
The Astrophysics of Emission-Line Stars
ASSL
Springer

Astrophysics of Emission-line Stars, pdf on web!!

http://books.google.am/books?id=Fyj8IQoZbLUC&printsec=frontcover&dq=kam-ching+leung&source=bl&ots=Tr3zWn8Kkk&sig=YgDgn2vPUy4Bey63Ftzygye2iQM&hl=hy&ei=pMqQTI24M8SUswaRoYG2AQ&sa=X&oi=book_result&ct=result&resnum=10&ved=0CDQQ6AEwCQ#

The Astrophysics of Emission-Line Stars

The books has 537 pages

Contents

Astrophysics of Emission-Line Stars

This presentation is concentration on

Part II Emission-Line Stars

H-R diagram and distribution of main emission-lines stars

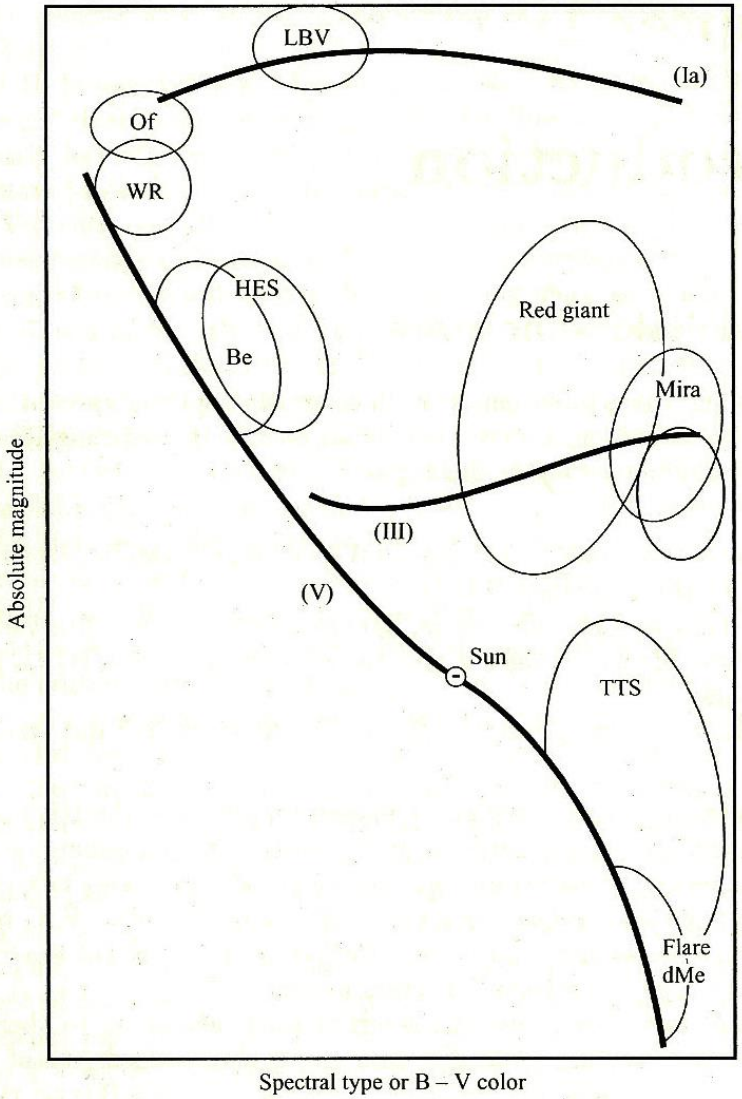

Figure 1.1: HR diagram and distribution of main emission-line stars.

Type and Number Emission-line Stars

Table 1.4: Type and number of emission-line stars observed up to 1948 (from Joy 1948)

Type	Number of Stars
WR stars	80
Stars of combination spectra (symbiotic stars)	20
P Cygni stars	20
Be and Ae stars	700
Eclipsing stars (Algols and close binaries)	20
W Virginis variables (Cepheids with CaII emission)	5
SS Cygni stars (dwarf novae)	40
T Tauri variables	12
RV Tauri variables (Pulsating supergiants)	30
Stars with bright H and K (stars with chromospheric activity)	150
Stars in dark lanes (T Tau-like stars)	40
Faint M stars (dMe)	40
Long-period variables (Mira variables)	3000
Total	4157

Note: Additional explanation is given in the brackets.

H-R diagram and distribution of main emission-lines stars

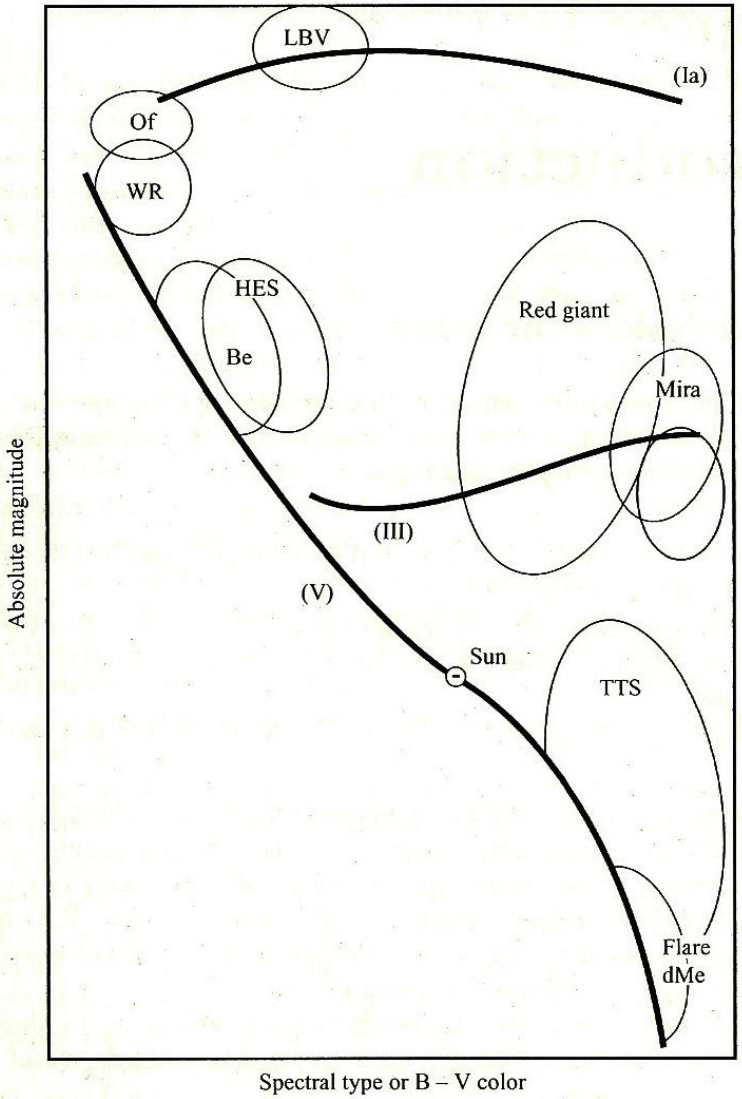

Figure 1.1: HR diagram and distribution of main emission-line stars.

EMISSION LINES ARE GENERALLY CLASSIFIED INTO TWO TYPES:

1. PERMITTED LINES
2. FORBIDDEN LINES

PERMITTED LINES

Transition from upper to lower energy levels through electric dipole radiation

FORBIDDEN LINES

Downward transitions are prohibited by the selection rules of transition and only possible through the electric quadrupole or magnetic dipole radiation with very small probabilities

WR Stars

Early-type

I. Wolf-Rayet stars

(i) The spectrum consists almost wholly of emission lines on the O-type continuum. Sometimes absorption lines appear at the violet edges of emission lines.

Early-type Wolf-Rayet stars

(ii) The emission lines are very broad. Interpreted as Doppler broadening, the widths correspond to thousands of km/sec and not necessarily the same for all lines.

Early-type Wolf-Rayet stars

(iii) The lines represent a wide range of excitation and ionization even in any one stars. The excitation level is generally much higher than that estimated from its color temperature of the continuous spectrum.

Early-type Wolf-Rayet stars

(iv) The spectrum falls into three groups due to the appearance of C, N, and O lines:

- WN stars
- WC stars
- WO stars

Main Emission Lines in WR Stars

NIII—λ4634–4641 Å (blend), λ5314 Å
NIV—λ3479–3484 Å (blend), λ4058 Å
NV—λ4603 Å, λ4619 Å, and λ4933–4944 Å (blend)
CIII—λ5272 Å, λ5696 Å
CIV—λ4650 Å, λ5805 Å, λ5470 Å, λ4684 Å
OV—λ4159 Å, λ5592 Å
OVI—λ3834 Å, λ3811 Å, λ5290 Å
HeII—λ4686 Å, λ5412 Å
HeI—λ5876 Å

Table 5.1 shows the classification criteria based on these emission lines for WN, WC, and WO, separately (van der Hucht 1992, Kingsburg et al. 1995). In this table inequality denotes the relative strength of emission lines. For WO group, the revised classification scheme by Kingsburg et al. (1995) is adopted.

Spectral Classification of WR Stars

Table 5.1: Spectral classification of WR stars (van der Hucht 1992, Kingsburg et al. 1995)

(1) WN sequence	Nitrogen emission lines	Other emission lines
WN2	NV weak/absent, NIV absent	HeII strong
WN3	NIV $\ll$ NV, NIII weak/absent	
WN4	NIV $\sim$ NV, NIII weak/absent	
WN5	NIII $\sim$ NIV $\sim$ NV	
WN6	NIII $\sim$ NIV, NV weak	
WN7	NIII $>$ NIV, NIII $<$ HeII 4686 Å	HeI weak (P Cyg profile)
WN8	NIII $\gg$ NIV, NIII $\sim$ HeII 4686 Å	HeI strong (P Cyg profile)
WN9	NIII strong, NIV weak NIIweal/abs.	HeI (P Cyg profile)
WN10	NII $\sim$ NIII, NIV absent	Balmer line, HeI (P Cyg profile)
WN11	NII strong, NIII absent, NIV absent	Balmer lines, HeI (P Cyg profile)
(2) WC sequence	Carbon emission lines	Other emission lines
WC4	CIV strong, CII weak/absent	OV intermediate
WC5	CIII $\ll$ CIV	CIII $<$ OV
WC6	CIII $\ll$ CIV	CIII $>$ OV
WC7	CIII $<$ CIV	CIII $\gg$ OV
WC8	CIII $>$ CIV	CII absent, OV weak/absent
WC9	CIII $>$ CIV	CII weak, OV weak/absent
(3) WO Sequence	Oxygen emission lines	Other emission lines
WO1	OVI $\gg$ OV, no OIV	OV $\gtrsim$ CIV
WO2	OVI $>$ OV, no OIV	OV $<$ CIV
WO3	OVI $>$ OV, OVI $>$ OIV	*OV* $\ll$ CIV
WO4	OVI $>$ OV, OVI $\approx$ OIV	*OV* $\ll$ CIV
WO5	OVI $>$ OV, OVI $\approx$ OIV	OV $\ll$ CIV

There two major groups of WR stars:

(i) Classical WR stars, pop I stars, high masses & luminosities

(ii) Central stars of planetary nebulae, pop II stars, low masses & luminosities

Mass Ratio and Spectral-type of WR Stars

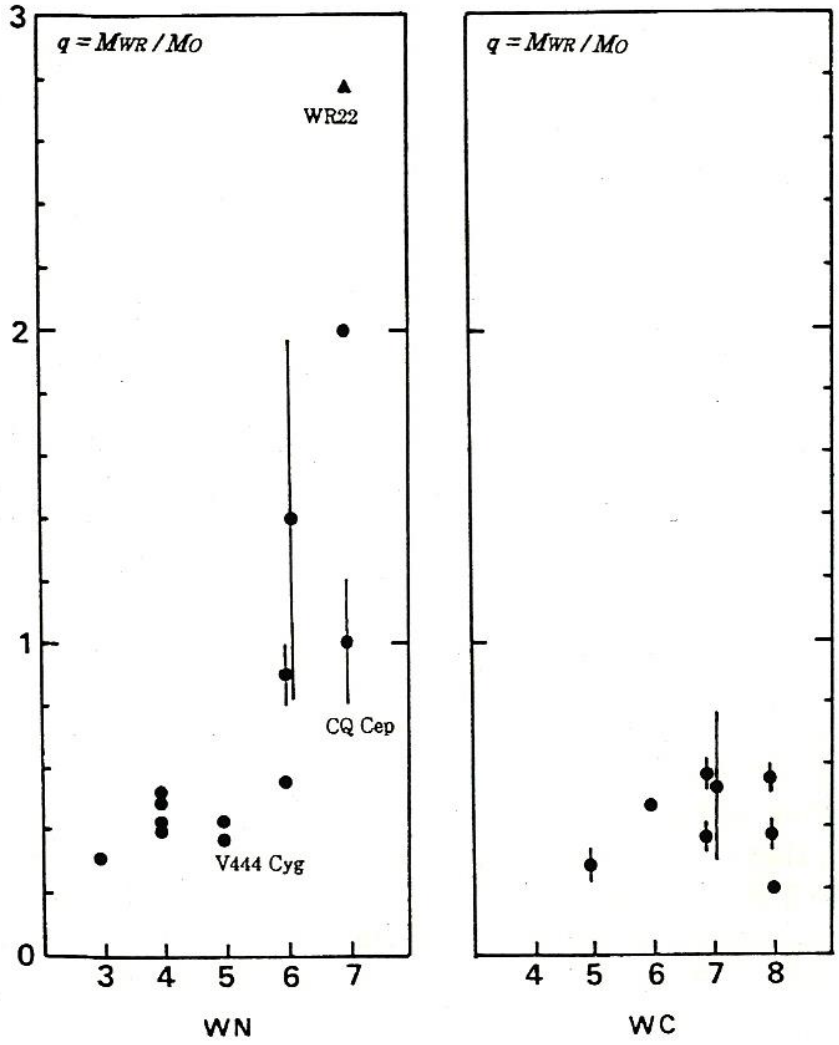

Figure 5.11: Correlation between mass ratio and the spectral subtype of WR binaries. Data points are plotted based on Smith and Maeder (1989) and Rauw et al. (1996).

II. O-type Emission-line Stars

Classification O-type Emission-Lines Stars

1. Of Stars
2. Oe Stars
3. PNCS- Planetary Nebulae Central Stars

Spectral Features of Of Stars

Table 5.8: Spectral features of Of stars (adapted from Walborn 1971)

Types of stars/lines	NIII $\lambda\lambda$ 4634, 4640, 4642 Å	HeII λ 4686 Å	Number of stars
Of	Strong emission	Strong emission	16
O(f)	Emission	Absence or weak absorption	13
O((f))	Emission	Strong absorption	20

Note: The number of stars is taken from Conti and Leep (1974).

Line Profiles 0f Of Stars

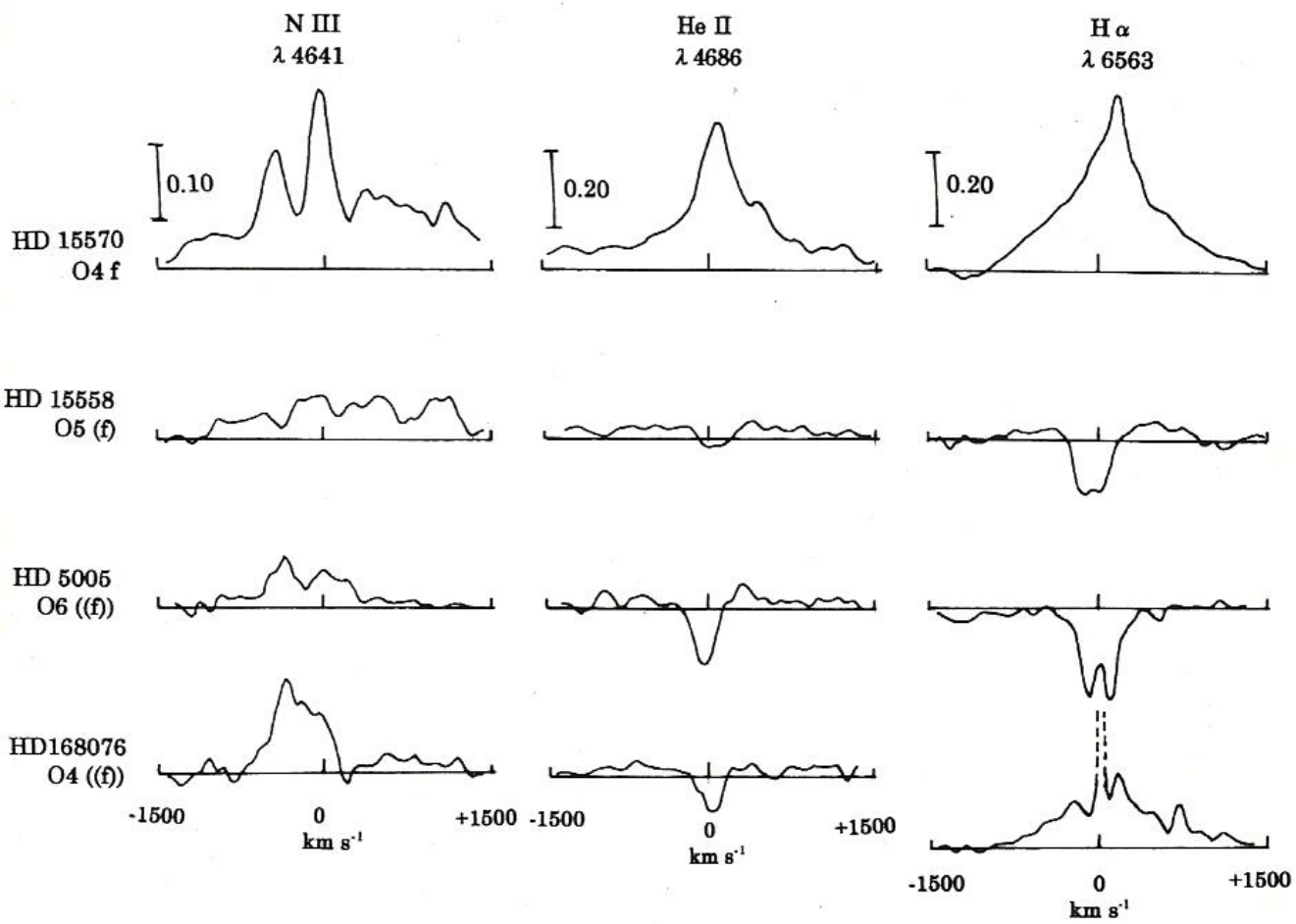

Figure 5.13: Comparison of three typical lines of Of spectra: Blended NIII (λ 4634, 4640, 4642 Å), HeIIλ 4686 Å, and Hα, are shown for four stars in different types of Of, O(f) and O(f)). Intensity scale is given in upper part. Profiles are schematically drawn based on the observations by Conti and Frost (1977).

Comparison of Rotational Velocity of Of and O Stars

Table 5.10: Comparison of average rotational velocity $V \sin i$ for Of and O stars (based on the data of Penny 1996)

Luminosity class	V–III			II–I		
	$\langle V \sin i \rangle$ (km s^{-1})	σ (km s^{-1})	N	$\langle V \sin i \rangle$ (km s^{-1})	σ (km s^{-1})	N
Of, O(f), O((f))	118	70	38	127	37	23
O	138	99	60	107	50	50

Note: N is the number of stars used.

Stellar Winds and Mass-loss Rate of Of Stars

Table 5.11: Stellar winds and mass-loss rates of Of stars (adapted from Lamers and Leitherer 1993)

Star HD	Name	Spectral type	Mass-loss Rates $\log\dot{M}(M_\odot \mathrm{yr}^{-1})$ (Hα)	(radio)	Terminal velocity V_∞ (km s^{-1})	V_∞/V_{esc}
14947		O5If+	−5.32	<-4.76	2300 ± 70	2.61
15558		O5III(f)	−5.61	—	3350 ± 200	3.60
15570		O4If+	−5.02	−5.33	2600	3.92
15629		O5V((f))	−5.77	—	2900 ± 70	2.79
24912	ξ Per	O7.5IIIn(f)	−5.89	—	2400 ± 100	2.70
36861	λ Ori	O8III((f))	−6.20	<-6.04	2400 ± 150	2.79
66811	ζ Pup	O4I(n)f	−5.45	−5.62	2200 ± 60	2.27
151804		O8Iaf	−5.00	−5.00	1600 ± 70	2.50
188001	9 Sge	O7.5Oaf	−5.38	—	2950 ± 150	2.86
190429A		O4 If	−5.16	—	2300 ± 70	2.50
210839	λ Cep	O6I(n)fp	−5.46	−5.68	2100 ± 60	2.53

Oe Emission-line Stars

Oe stars are O-type stars that show emission lines in Balmer series. In contrast to Of stars, they do not show emission lines in high excited ions such as NIII and HeII.

They may interpreted as an extension of Be

PNCS

Central Stars of Planetary Nebulae, PNCS

The central stars of planetary nebulae consists of hot, dwarf stars with diversity in spectral types such as; [WR], Of, Of+[WR], OVI, O-type, subdwarf O stars, etc.

III. Classification of B-type Emission-Line Stars

1. Be Stars- Classical Be Stars

2. B[e] Star-IR Excess & Appearance of Forbidden Lines

Basic Type of Line Profiles and Catalogues of Be Stars

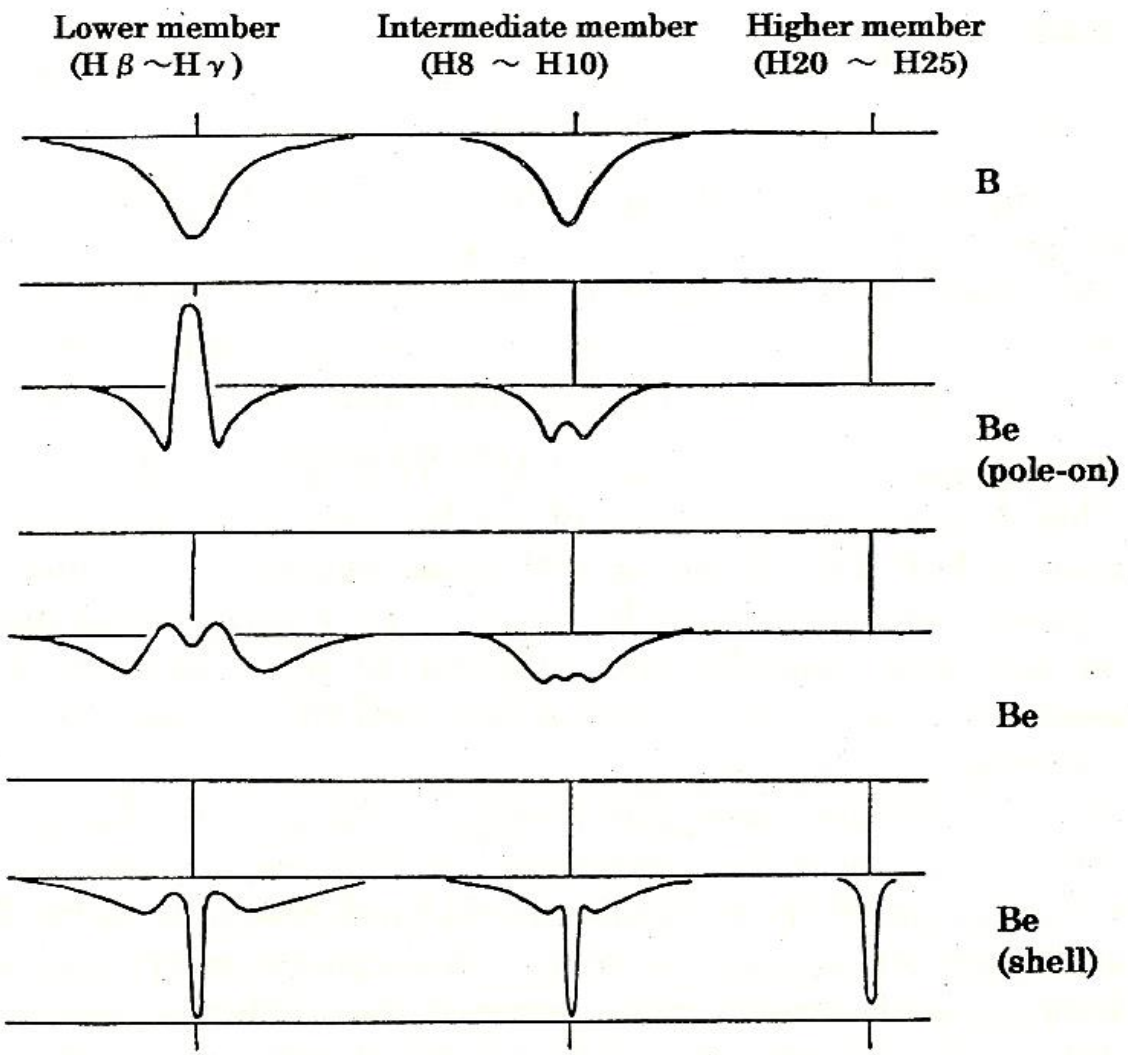

Figure 5.16: Typical schematic profiles of B and Be stars.

Schematic Diagram of Classical Be Star

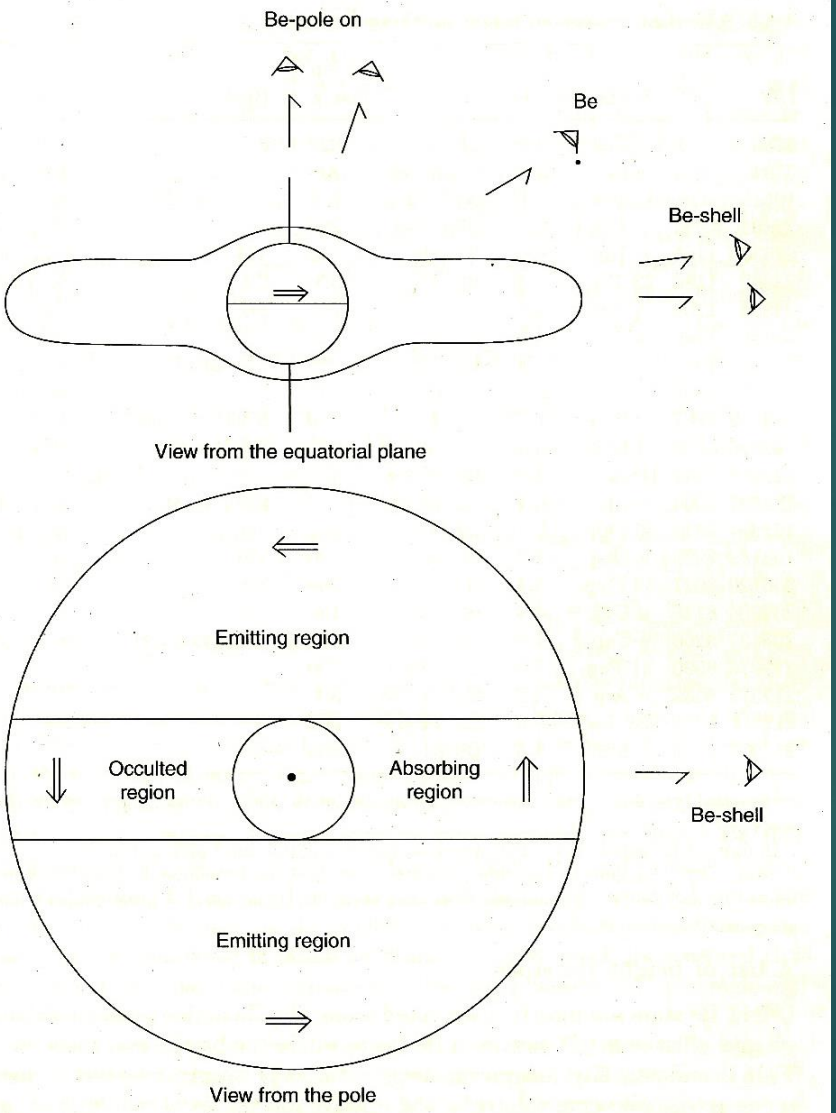

Figure 5.17: Classical model of rotating envelope of Be stars and the types of Be star emission-line profiles originally proposed by Struve (1931).

High Rotational Velocity among Be Stars

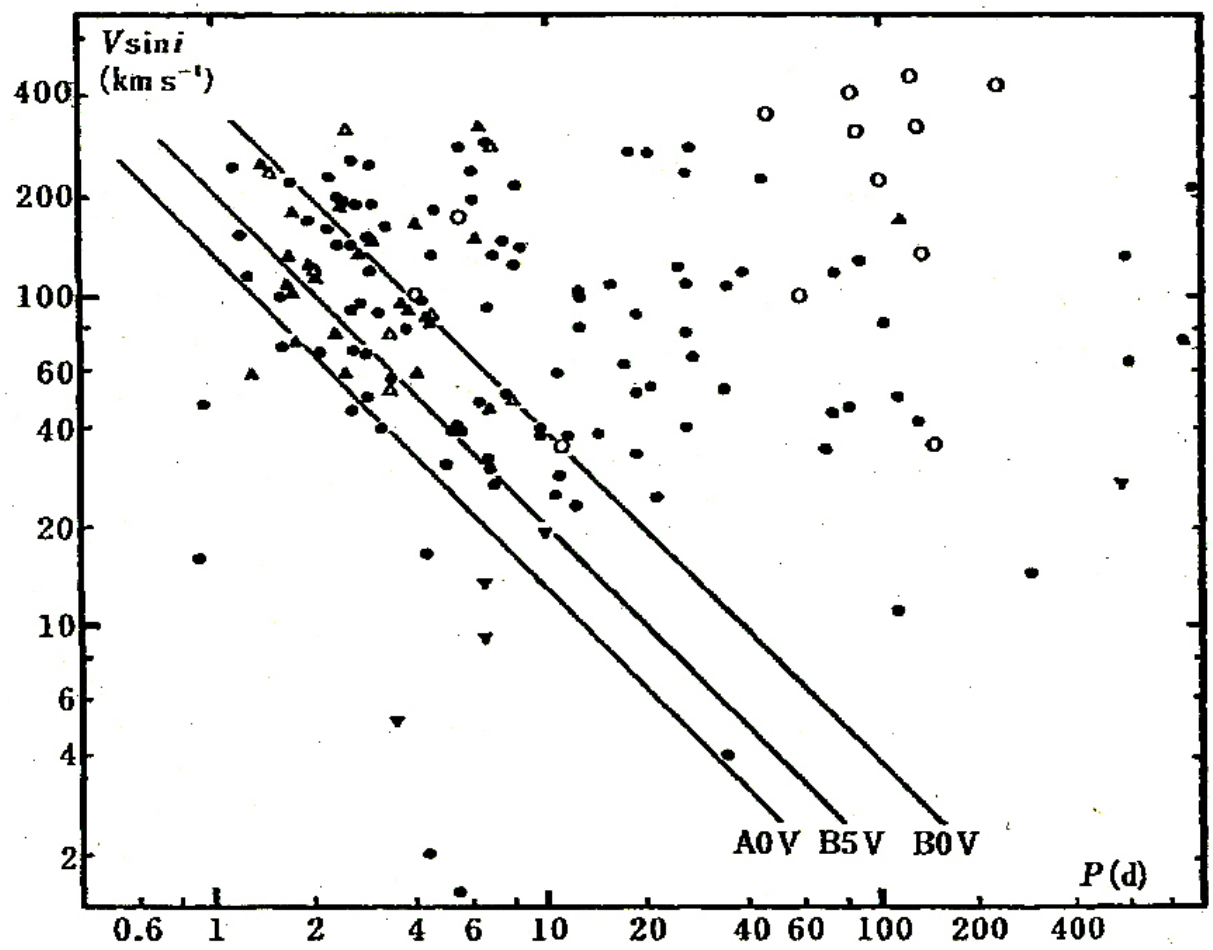

Figure 5.18: The period-rotational velocity relation for the spectroscopic binaries of B0–B9, V–III. Circles and triangles denote the noneclipsing and eclipsing binaries, respectively. The inverted triangles denote Bp stars. The emission-line stars are designated by open marks in each case. The lines of synchronization between axial rotation and orbital motion are also shown (Kogure 1981).

Break-up Velocity and Be Stars

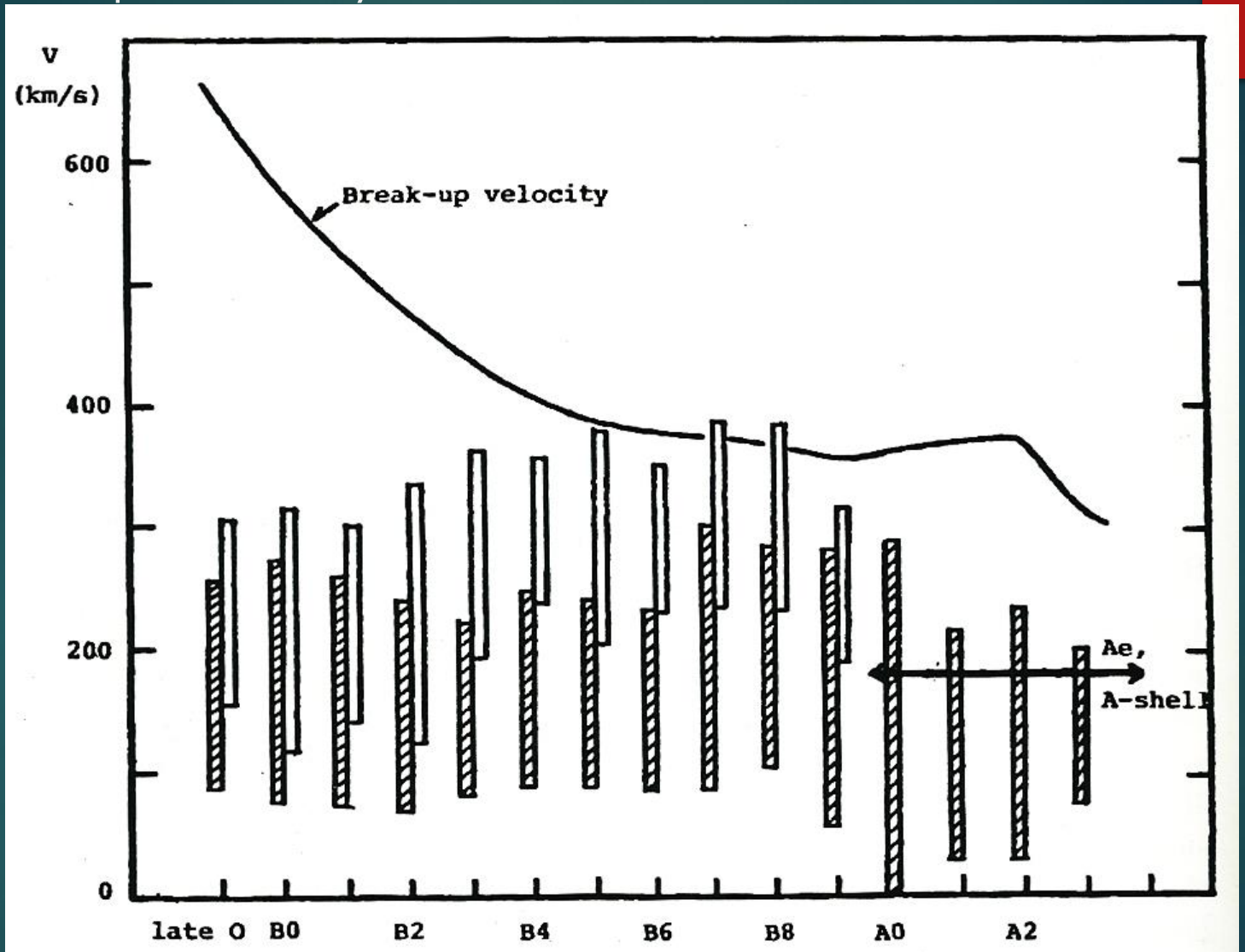

Figure 5.19: The distribution of rotational velocity V in km s^{-1} is shown along the

Approaching Break-up Velocity of Be Stars

Table 5.16: Average values of $V \sin i$, number of stars, and ratio of $\langle V \rangle / V_c$ for different spectral subtype and different luminosity class of classical Be stars (adapted from Yudin 2001)

Luminosity class	III, III–IV				
Spectral subtype	O–B1.5	B2–B2.5	B3–B5.5	B6–B9.5	O–B9.5
Number of stars	37	30	28	40	135
$\langle V \sin i \rangle$	203 ± 11	211 ± 10	192 ± 14	207 ± 10	201 ± 6
$\langle V \rangle / Vc$	0.57	0.66	0.64	0.83	0.67
Luminosity class	IV–V, V				
Spectral subtype	O–B1.5	B2–B2.5	B3–B5.5	B6–B9.5	O–B9.5
Number of stars	66	78	78	61	283
$\langle V \sin i \rangle$	202 ± 9	207 ± 8	236 ± 7	243 ± 7	229 ± 4
$\langle V \rangle / Vc$	0.49	0.55	0.67	0.78	0.63

Note: Vc is the critical velocity defined by Equation (5.3.3).

Much higher value of $\langle V \rangle / V_b = 0.95$ has been obtained by Townsend et al. (2004) by taking into account the effects of the von Zeipel gravity darkening law ($T_{\rm eff}^4 \sim g_{\rm eff}$) in rapidly rotating stars. Thus they claimed that Be stars may be rotating much closer to their critical velocities than is generally supposed. If Be stars are actually rotating at or near the critical velocities, the dynamical processes responsible for the formation and development of Be envelopes should be affected seriously.

Mass-loss Rate and luminosity of Be Stars

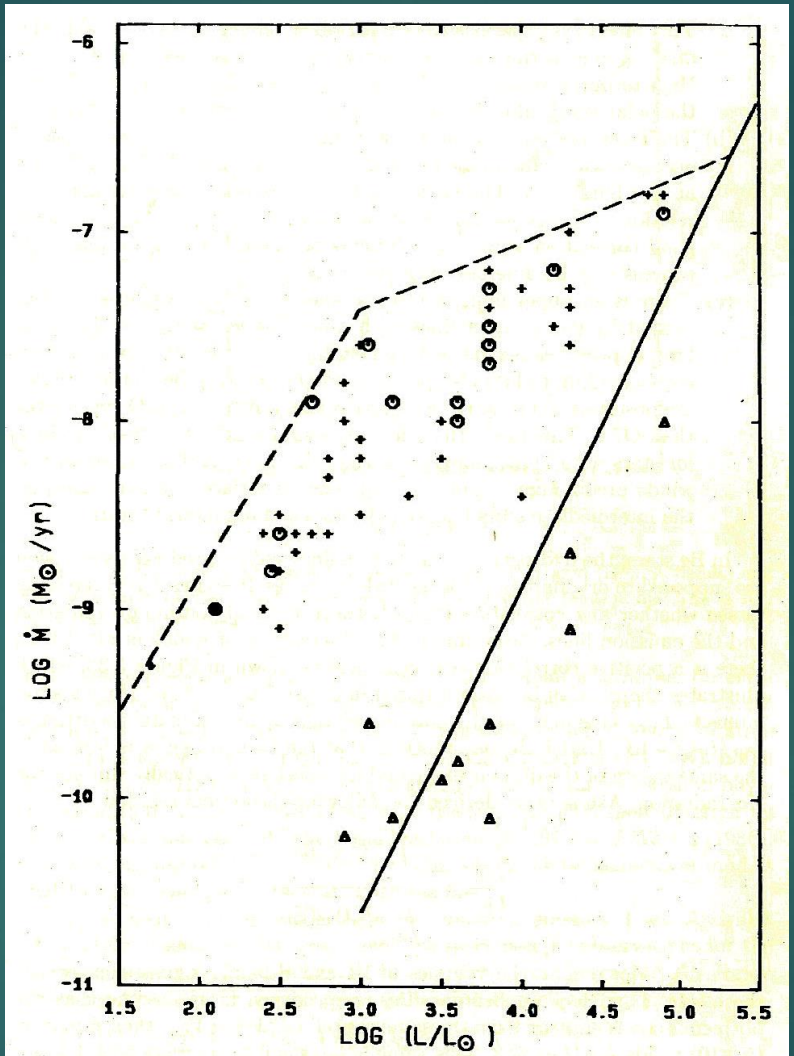

Figure 5.32: The mass loss-luminosity diagram for Be stars. Circles are the stars observed with 12, 25, and 60 μm IR bands, pluses the ones with 12 and 25 μm data. The dashed line is the upper limit for $\dot{M}_{\rm IR}$. Triangles are the mass-loss rates derived by Snow (1981) based on the profiles of UV resonance lines. The solid line gives extrapolation of the $(\dot{M}, L)$ relation for luminous O type stars. (From Waters et al. 1987)

Ratio of X-ray and Bolometric Luminosity of Be Stars

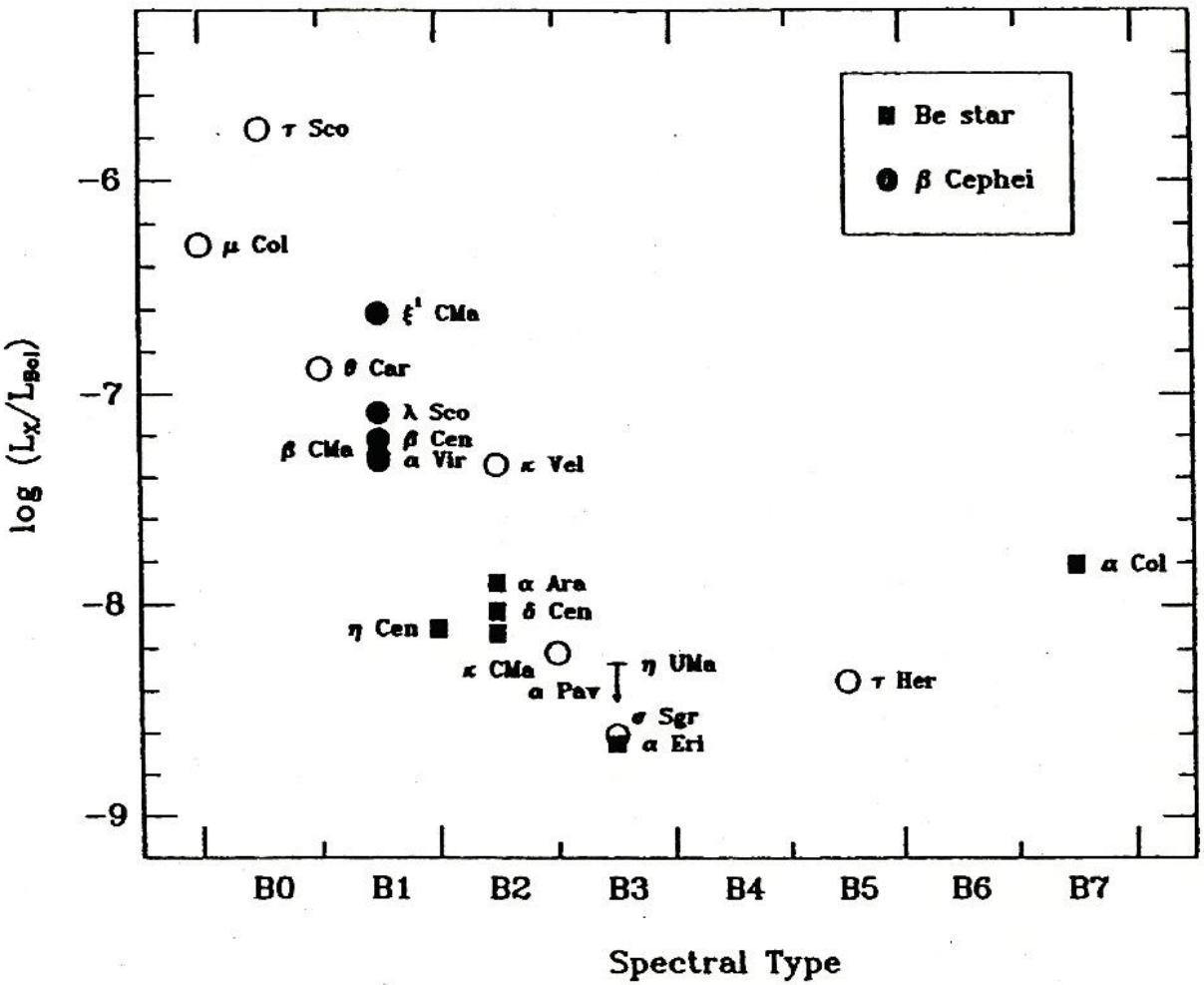

Figure 5.35: The relation between the ratio of X-ray luminosity to bolometric luminosity and the spectral type of B stars. Stars are designated by open circles for B stars, filled circles for β Cephei and filled squares for Be stars. (From Cassinelli and Cohen 1994)

Groups of Peculiar Be Stars

Table 5.20: Groups of peculiar Be stars and sample stars

Group	IR excess $H-K$	Emission lines: Permitted	Emission lines: Forbidden	Number of stars	Sample Stars
1	0.7–2.0	Weak emission in Balmer, FeII	[OI]	17	HD 31648 HD50138 HD163296
2	1.0–2.3	Strong emission	Numerous, [FeII],[OI], etc.	26	HD45677 MWC645 MWC349
3	0.4–2.2	High excitation	[OIII], [NeIII] Similar to PN with high excitation (>25 eV)	22	HD51585 HD316248 HD167362

Note: The H–K color takes the values of $-0.1 \sim +0.5$ in ordinary Be stars (Allen and Swings 1976).

IV. Supergiant Emission-line Stars
Types of Luminous Blue Variables

Type 1: The large variations with $\Delta V \geqq 3$ magnitudes, associated with eruptive ejection of a large amount of mass. The time scale between large outbursts is very long over centuries, e.g., η Car, P Cyg.

Type 2: The moderate variations of $\Delta V \sim 1$ magnitude, the time scale is of the order of decades, e.g., AG Car, S Dor.

Type 3: The small-scale irregular variations with $\Delta V \sim 0.1$–0.2 magnitude, occurring on time scales of weeks to months. This type of variations is common among LBVs.

HR Diagram of Luminous Blue Variables

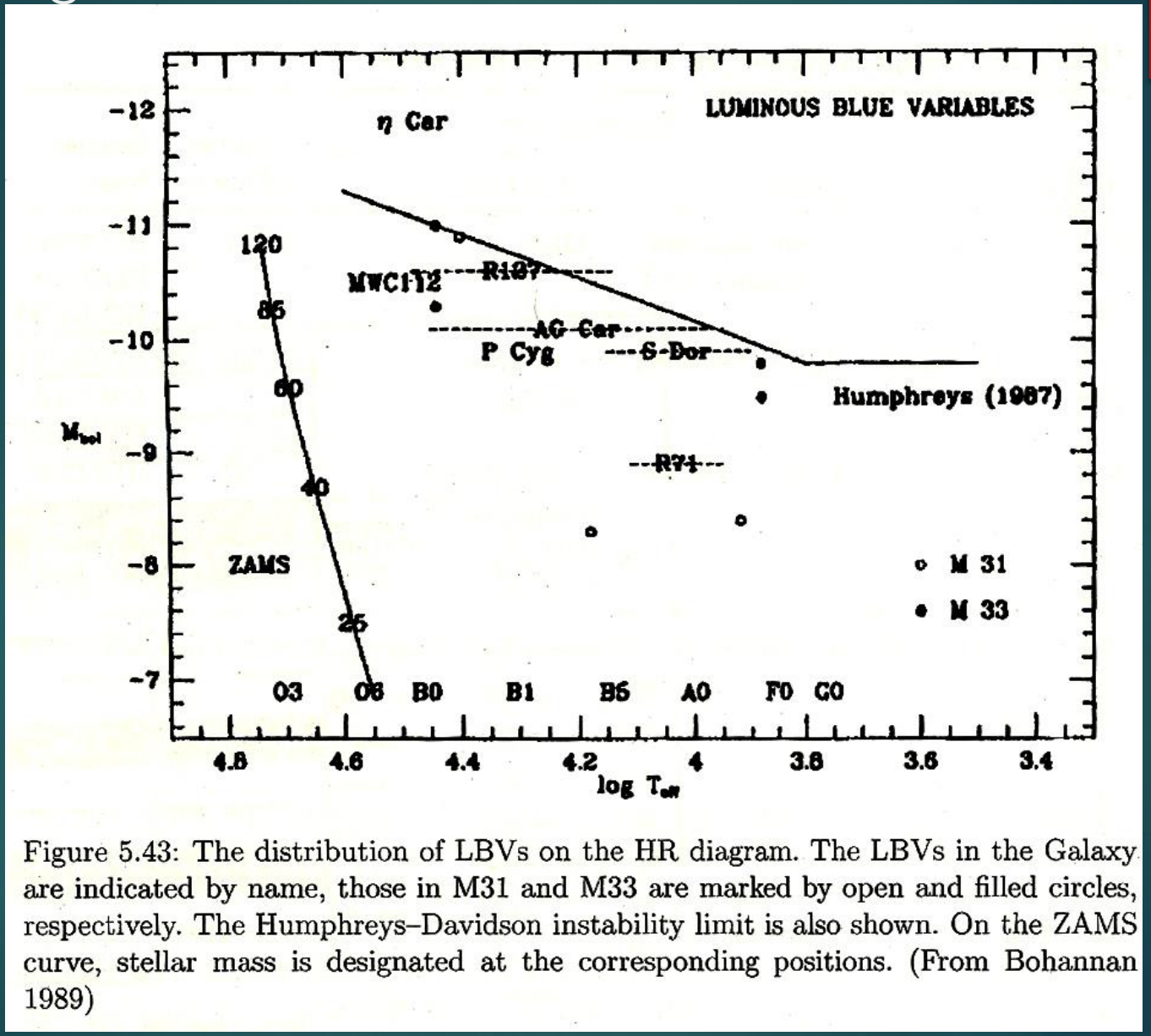

Figure 5.43: The distribution of LBVs on the HR diagram. The LBVs in the Galaxy are indicated by name, those in M31 and M33 are marked by open and filled circles, respectively. The Humphreys–Davidson instability limit is also shown. On the ZAMS curve, stellar mass is designated at the corresponding positions. (From Bohannan 1989)

The Famous Eta Carini

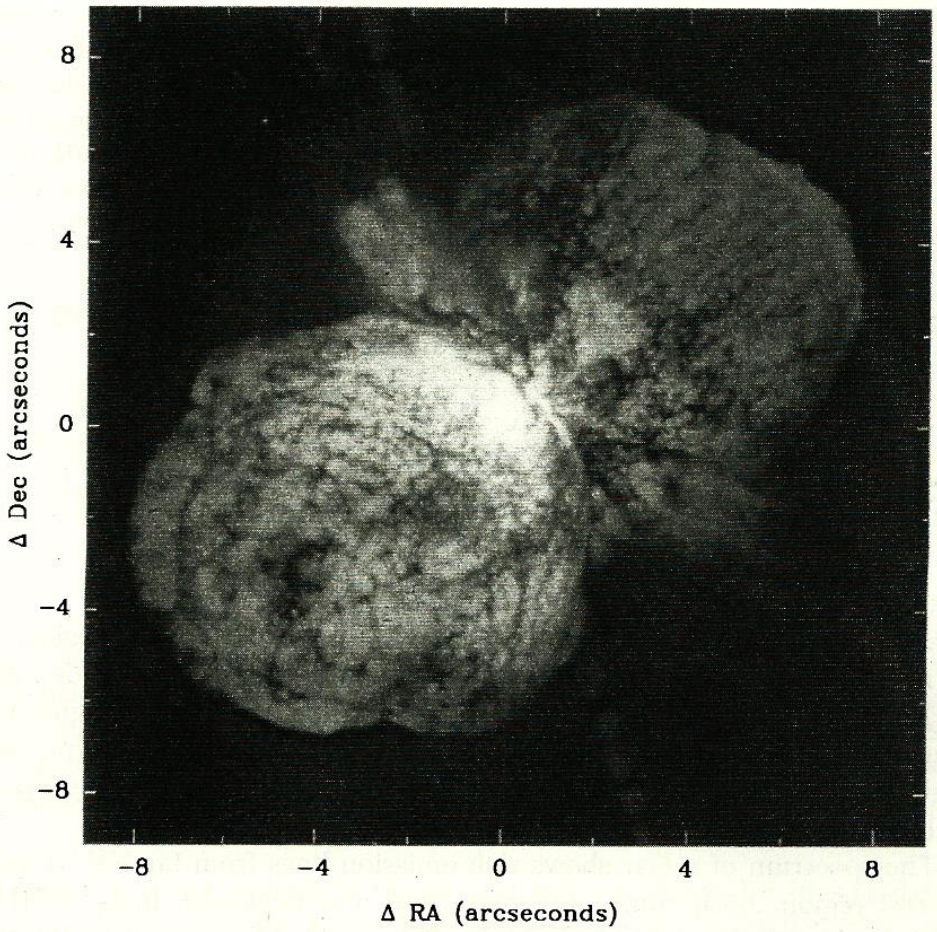

Figure 5.44: Nebulosity around η Car observed with the Planetary Camera (red band) of the HST in 1996. Two distinct lobes are visible on both sides of the unseen central star. In between two lobes, a giant thin equatorial disk is also seen. These lobes are supposed to be gas cloud ejected from the star at the time of great eruption in 1843. The scale $4''$ corresponds 5700 AU at the distance of η Car. (From Morse et al. 1998)

Schematic Diagram of Expanding Envelope of P Cygni Stars

P Cygni Stars

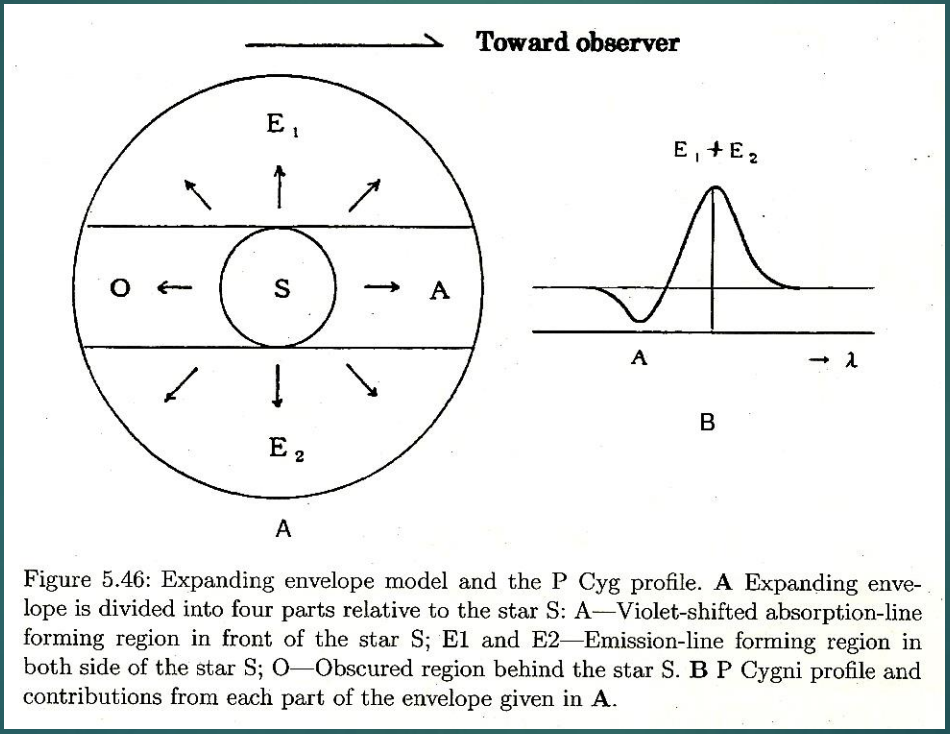

Figure 5.46: Expanding envelope model and the P Cyg profile. **A** Expanding envelope is divided into four parts relative to the star S: A—Violet-shifted absorption-line forming region in front of the star S; E1 and E2—Emission-line forming region in both side of the star S; O—Obscured region behind the star S. **B** P Cygni profile and contributions from each part of the envelope given in **A**.

Types of P Cygni Profile

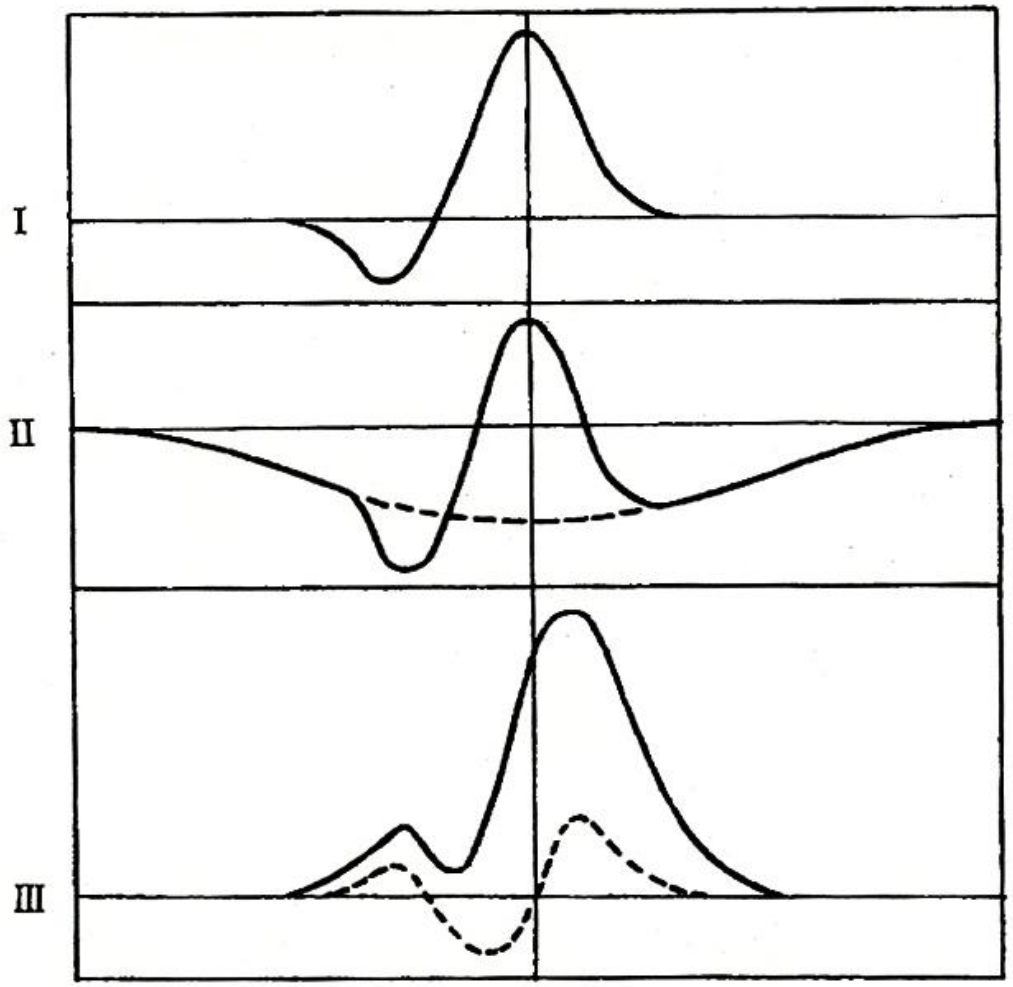

Figure 5.47: Types of P Cygni profile defined by Beals (1951).

HR Diagram of P Cygni-type Stars

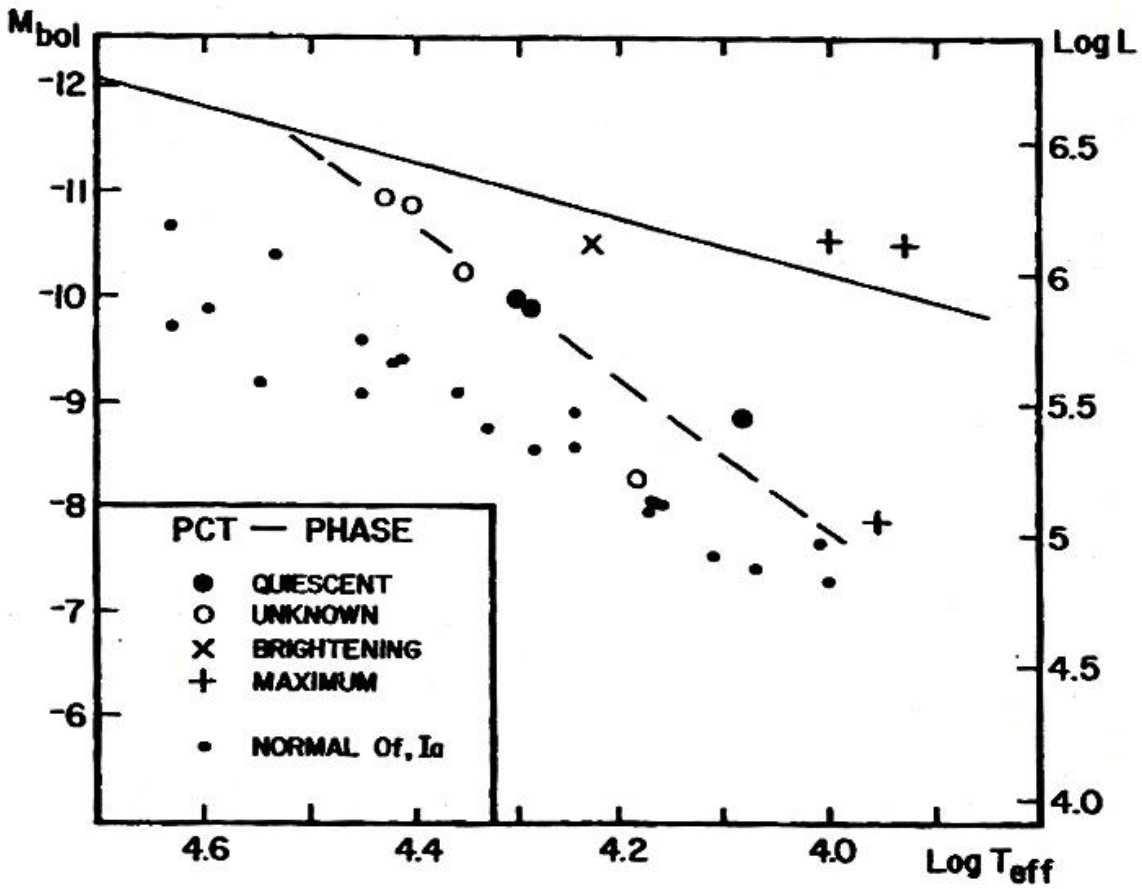

Figure 5.50: HR diagram of the P Cyg-type stars (PCT). Symbols indicate the phase of their activity as shown in the inserted box. The positions of Of stars and normal supergiants are shown by small filled circles for comparison. The solid line indicates the Humphreys–Davidson's upper limit, and the broken line gives the mean brightness for the quiescent phase of the PCT. (From Lamers 1986)

Characteristics of P Cygni-type Stars

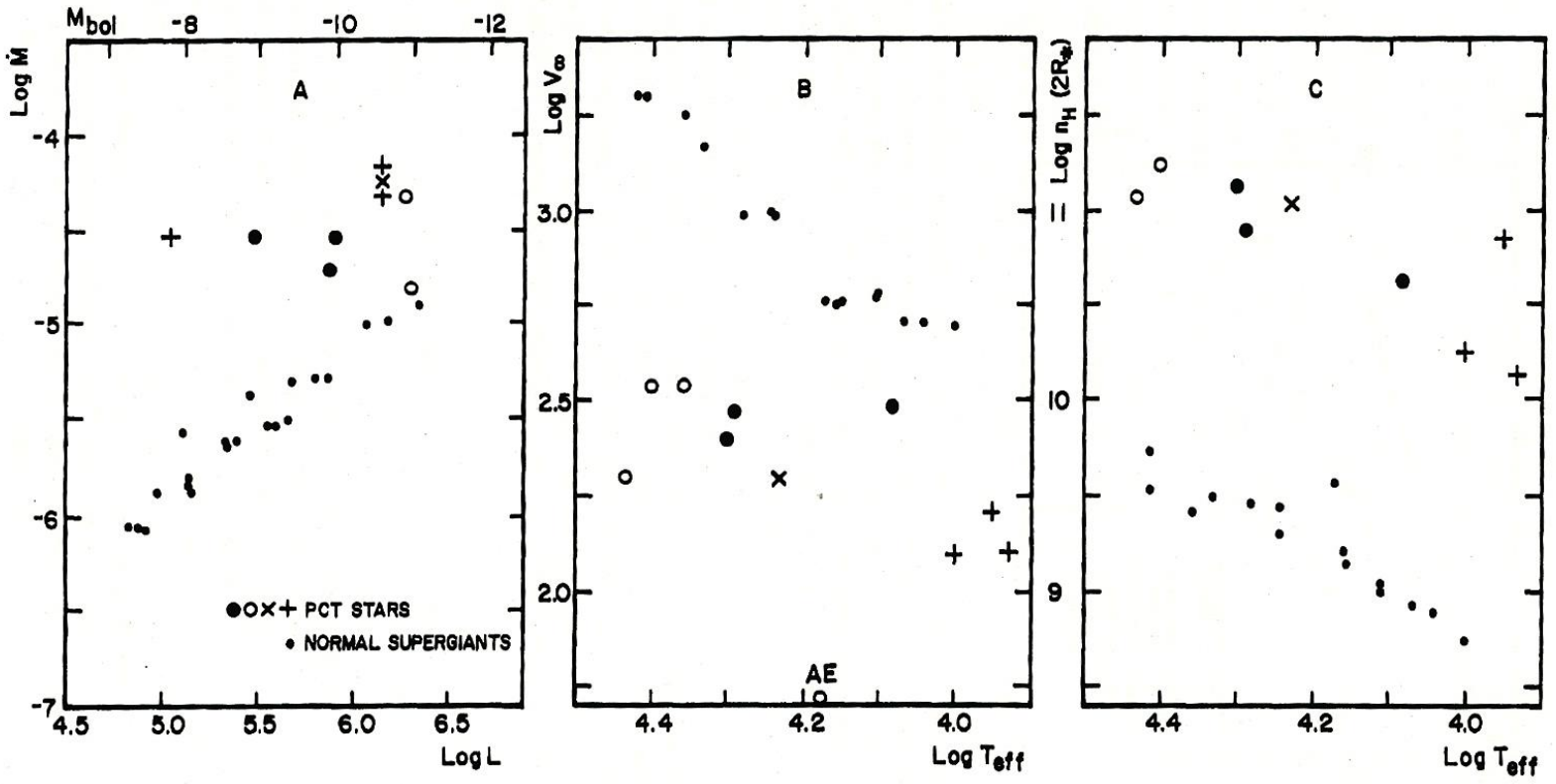

Figure 5.51: The mass-loss characteristics of the P Cyg-type stars compared to those of normal supergiants. **A**: Mass-loss rate $\dot{M}(M_\odot$ per year) versus stellar luminosity L. **B**: Terminal velocity V_∞ (km s^{-1}) versus effective temperature $T_{\rm eff}$. **C**: Gas density of the wind n_H (cm^{-3}) at 2 R_* versus $T_{\rm eff}$. The symbols of stars are the same as in Figure 5.56. (From Lamers 1986)

Characteristics of Supergiant B[e] Stars

According to Zickgraf (1992), the spectra of sgB[e] stars are characterized by the following properties:

(a) Strong Balmer emission, frequently showing P Cygni profiles. The equivalent width of the Hα emission is as high as 10^2–10^3 Å.
(b) Appearance of narrow emission lines both of permitted and forbidden lines such as FeII, [FeII] and [OI].
(c) Strong infrared excess due to thermal radiation of hot dust envelope ($T_{\rm dust} \sim 1000$ K, $R_{\rm dust} \sim 300\ R_*$).

Hubble-Sandage Stars

Hubble-Sandage stars

Hubble and Sandage (1953) first paid attention to five extragalactic luminous variable stars, one in M31 (Var 19 = AF And) and four in M33 (Vars A, B, C, and 2). These five stars have become known as the Hubble-Ssndage variables (hereafter abbreviated as HS variables). Their characteristic features are as follows:

(1) They are irregular variables with the highest luminosity class in the galaxies.

(2) They show strong, hot continuum in the ultraviolet region.

(3) They show intermediate F-type spectra with strong emission lines in the Balmer and in some ionized metals.

Optical Spectra of Hubble-Sandage Stars

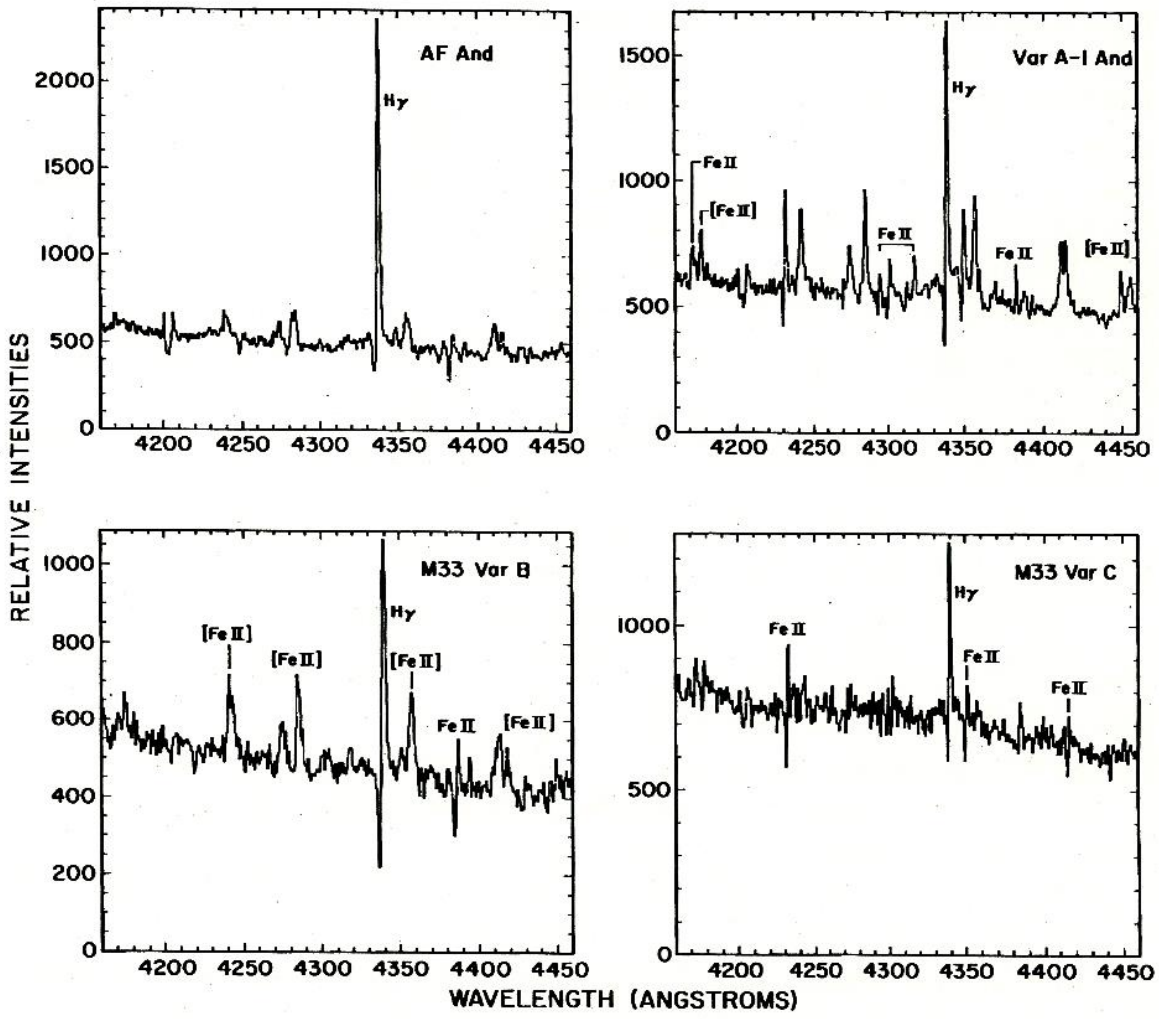

Figure 5.53: Optical spectra over λ 4160–4450 of the HS variables in M31 and M33. Spectral resolution is around 1 Å. P Cygni profiles are visible on the Hγ and some FeII lines. (From Kenyon and Gallagher 1985)

Physical Parameters of Hubble-Sandage Variables

Table 5.24: Physical parameters of the HS variables (adapted from Szeifert et al. 1996)

	Model parameters		Derived parameters			
Star	$T_{\rm eff}$ (K)	log g	$R_*/R_\odot$	V_∞ (km s^{-1})	log $L/L_\odot$	dM/dt($M_\odot$ per year)
AF And	30,000	3.2	63	150	6.5	$3\ 10^{-5}$
Var B	9,000	—	440	90	6.05	$3\ 10^{-4}$ (B) $4\ 10^{-5}$ (C)
Var C	13,000	1.6	185	80	5.9	$2\ 10^{-5}$

Note: The mass loss rate of Var B: (B) fitting with Balmer profile, (C) fitting with continuum.

Evolutionary Status of Early-type Emission-line Stars

Stars > 20 solar mass

Standard models

O→ Of → BSG (or H-rich WN) → LBV → WN → WC → SN

Dynamical processes models

O → Of → H-rich WN → LBV → H-poor WN → WN → WC → SN

Evolutionary Tracks of Massive Stars

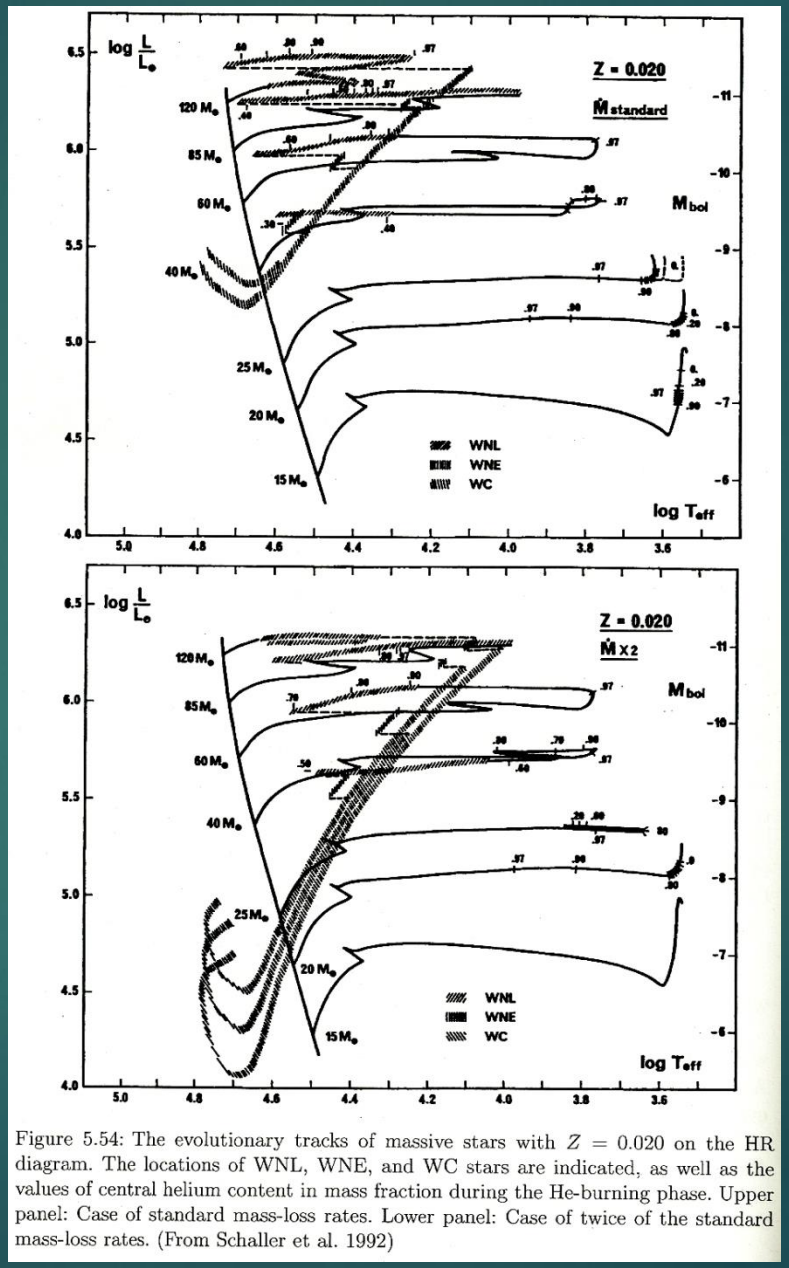

Figure 5.54: The evolutionary tracks of massive stars with $Z = 0.020$ on the HR diagram. The locations of WNL, WNE, and WC stars are indicated, as well as the values of central helium content in mass fraction during the He-burning phase. Upper panel: Case of standard mass-loss rates. Lower panel: Case of twice of the standard mass-loss rates. (From Schaller et al. 1992)

Evolution of Massive Stars

On the evolution of massive rotating stars, a remarkable progress has been made in late 1990s to early 2000s. Meynet and Maeder (2003) paid particular attention to WR star phase at solar metallicity. Based on revised model calculations, they showed the remarkable effects of rotation in the evolutionary tracks. For comparison we shall consider nonrotating stars ($V_{\rm ini} = 0\,{\rm km\,s^{-1}}$) and rotating stars ($V_{\rm ini} = 300\,{\rm km\,s^{-1}}$) with initial mass of 60 $M_\odot$, where $V_{\rm ini}$ denotes the initial rotation velocity at ZAMS.

(1) Evolutionary sequence. Nonrotation O stars evolve to WR stars through LBV stars, that is, through lower surface-temperature phase. In contrast, rotating O stars directly evolve to WN stars and then to WC stars, because of large mass-loss rate due to rotational instability.

(2) Lifetimes in WR stars. The WR stage of evolved O stars proceeds as

$$\text{WNL(late type WN)} \rightarrow \text{WNE(early type WN)} \rightarrow \text{WN/WC transition} \rightarrow \text{WC}$$

Total duration of this WR stage is 0.4 Myr in nonrotating stars, whereas it takes 0.75 Myr in rotating stars.

(3) Surface abundance in WR stars. Initial cosmic abundance of O stars changes to CNO equilibrium abundance at WN stars, and to C abundant phase in WC stars. This change occurs much gradually in rotation stars as compared to nonrotation stars. This age dependence of surface abundance reflects to the population of WR stars in each phase of WNL, WNE, WN/WC, and WC, which can be compared with observed population of WR stars.

Evolution of Be Stars, 1

The origin of single Be stars has long been discussed in connection with the distribution of Be stars on the HR diagram. Three different views have so far been proposed.

(1) The first view is that the Be phenomenon occurs during the overall contraction phase that follows the exhaustion of hydrogen in the core (Schild and Romanishin 1976). In this case, one would expect that Be stars appear near the end of the main sequence phase, i.e., Be stars should be brighter than normal B stars as a whole. This view was supported by Singh and Chaubey (1987) based on their photometric data for the distribution of Be stars on the HR diagram.

Evolution of Be Stars, 2

(2) The second view is that Be stars are the particular phenomena temporarily appearing among rapidly rotating B stars at any point in the main-sequence lifetime. Zorec and Briot (1997) selected B and Be stars of luminosity classes V–III from the BSC, and studied the frequency of Be stars, $P(\mathrm{Be}) = N(\mathrm{Be})/(N(\mathrm{B}) + N(\mathrm{Be}))$ for each spectral subtype and luminosity class, based on the two dimensional BCD classification. They thus found that $P(\mathrm{Be})$ takes two maximum values at B1 and B7 along the spectral subtype, regardless the luminosity class of stars. They suggested that Be stars hardly represent a given stage in the evolutionary track of every B star. In order to see the distributions of B and Be stars in the HR diagram, observations of open clusters are important. Slettebak (1985) constructed the HR diagram for 12 clusters, among which two clusters NGC 3766 and NGC 4755 in southern sky are shown in Figure 5.55. These clusters contain sufficient number of Be stars among their observed clusters. One may see in this figure that the Be stars are well mixed with B stars above the ZAMS. Feinstein (1987, 1990) also considered the characteristics of 124 Be stars in 52 open clusters on the color–magnitude diagrams in support of the conclusion of Slettebak.

Evolution of Be Stars, 3

(3) The third view is to claim the evolutionary effect that appears in the second half of the main-sequence lifetime of a B star. Fabregat and Torrejón (2000) showed the incidence of Be stars in open clusters as a function of the cluster age, i.e., the clusters younger than 10 Myr are almost completely lacking classical Be stars, and the maximum frequency P(Be) reaches in the age interval 13–25 Myr. They interpreted the Be phenomena as to be related to main structural changes happening at the later half evolutionary phase of B stars through the surface enrichment of helium abundance. According to Fabregat and Torrejón, the semiconvection or turbulent diffusion, which is responsible of the surface helium enrichment, is coupled with the high rotational velocity to generate magnetic fields via the dynamo effect and thereby originate the Be phenomena.

H-R Diagrams of Be and B Stars

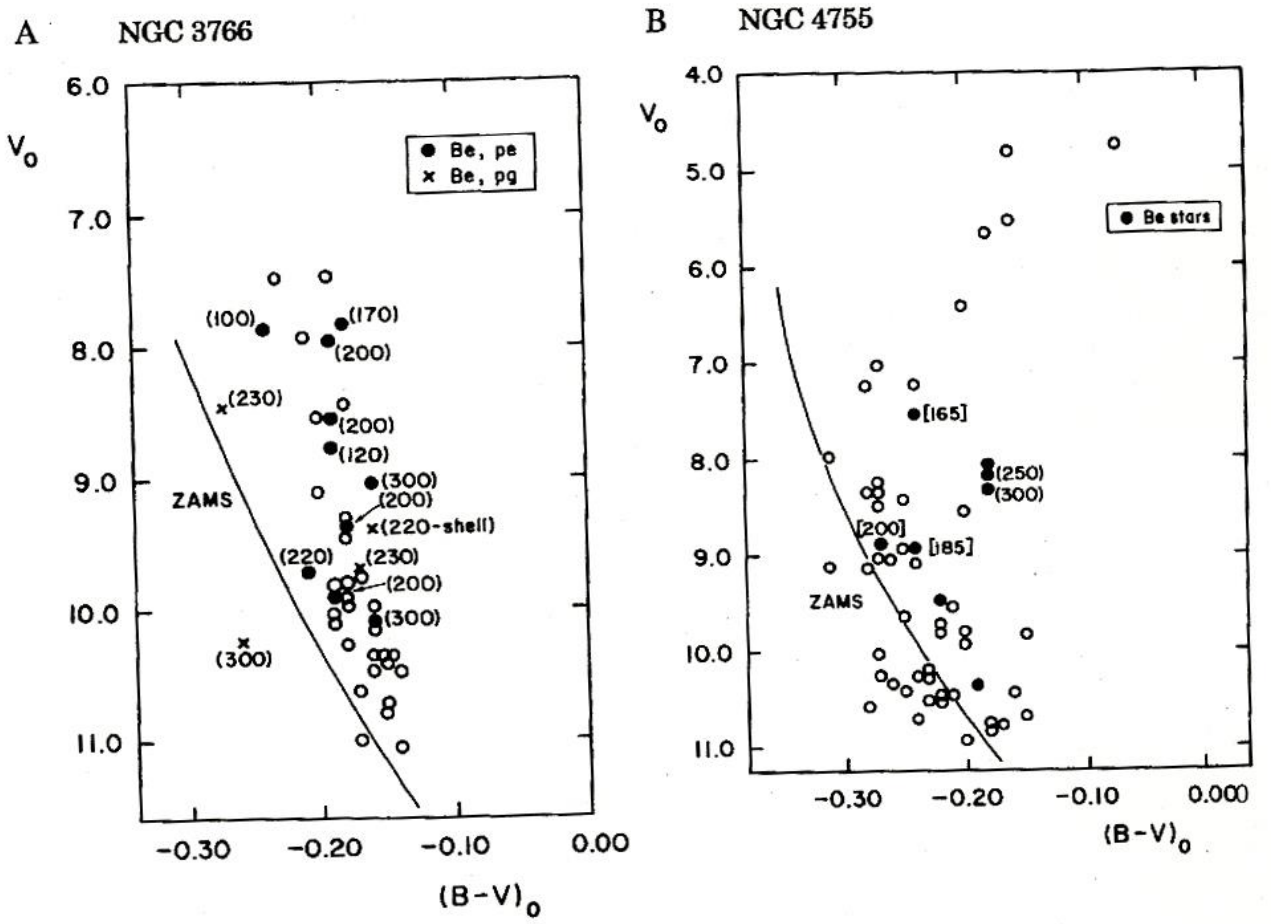

Figure 5.55: Color-magnitude diagram for open clusters. **A**. NGC 3766 (distance = 1.70 kpc, age = 22 Myr). **B**. NGC 4755 (distance = 2.34 kpc, age = 7 Myr). The abscissa denotes the intrinsic color index, the ordinate the V magnitude. The solid line indicates the ZAMS, filled and open circles give the Be and B stars, respectively. The figures in parenthesis in some stars denote the values of $V \sin i$ of that star. (From Slettebak 1985)

Schematic Binary Evolution Sequence

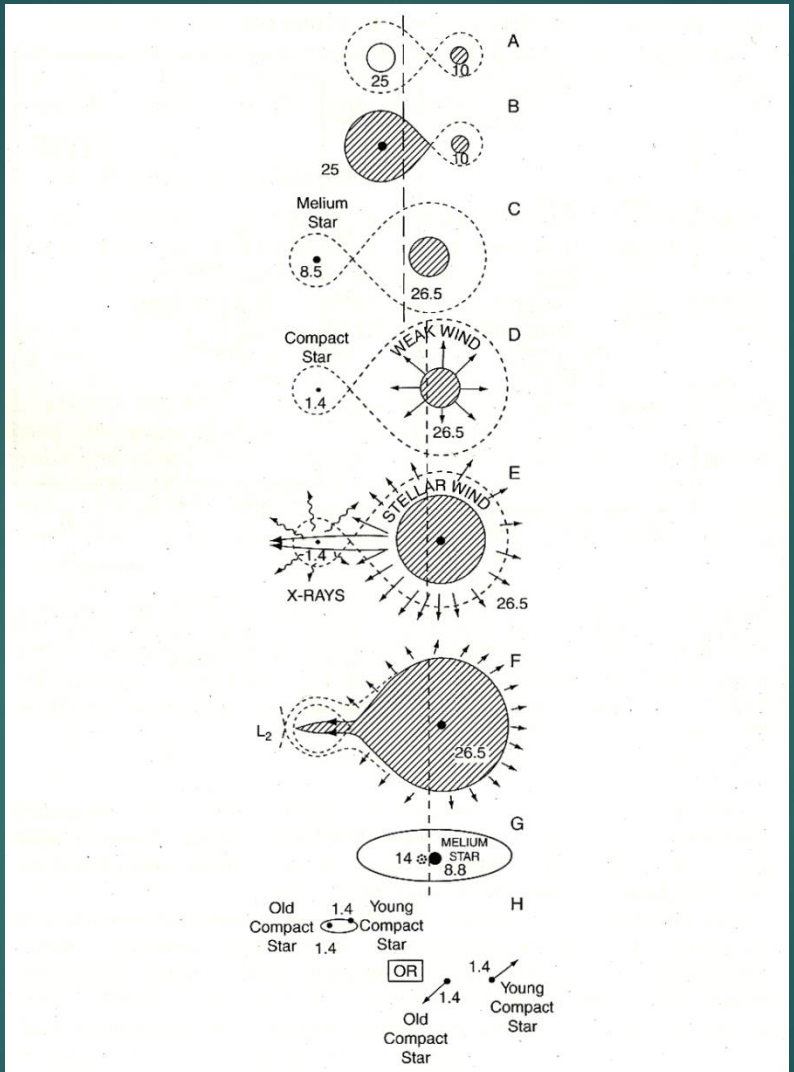

Figure 5.56: Evolution of a close binary system with initial mass of 25 and 10 $M_\odot$ and orbital period 5 days. Some typical steps are illustrated from (A) to (H), for each step the duration, binary state, and masses of component stars are given below. The system becomes a wind-powered HMXB (high mass X-ray binary) for some 10^4 years in step (E). Whether the system remains as a binary or disrupted in the final stage (H) depends on the fraction of mass-loss from the system. (From van den Heuvel 1994)

Binary Evolutionary life-time

Table 5.25: Main features of each step in Figure 5.56 (adapted from van den Heuvel 1994)

Step	Duration t (yrs) from ZAMS	Orbital period $P(d)$	Mass of components $M_1/M_\odot$	$M_2\ M_\odot$	Binary state
(A)	0	5.0	25	10	ZAMS
(B)	4.71×10^6	5.0	25	10	Start of RLOF
(C)	4.72×10^6	6.84	8.5	26.5	He star + WR?
(D)	5.2×10^6	11.9	1.4	26.5	He star to compact star through SN
(E)	9.00×10^6	11.9	1.4	26.5	M_2 star to supergiant with strong wind
(F)	9.01×10^6	11.9	1.4	26.6	RLOF from M_2 star
(G)	9.02×10^6	0.2	1.4	8.8	M_2 star to helium star binary or disruption.
(H)	9.5×10^6	—	1.4	1.4	

Evolutionary Scenario of Case B Binary System

In Table 5.26 evolutionary scenario of a close binary system and its possible observational counterparts are summarized in the subsequent phases (a) through (e). The initial step is the main sequence binary with masses of M_1^0

Table 5.26: Evolutionary scenario for case B close binary system. Based on Pols et al. (1991)

Step	Binary type	State and counterpart	Example
(a)	Unevolved detached MS + MS binary	B-type spectroscopic binary	
(b)	Semidetached binary with mass transfer	(RLOF phase) Be + cool companion	β Lyr, KX And
(c)	Detached binary spun-up B star + He star	Spectroscopic Be star	φ Per, HR2142(?)
(d)	Case of $M_1^0 > 10$ M. detached binary	Be star + NS classical Be /X-ray binary	X Per
(e)	Case of $M_1^0 < 10$ M. detached binary	Be star + WD low-luminosity Be/ X-ray binary	48 Per? κ Dra(?)

Note: RLOF, Roche lobe overflow; NS, neutron star; WD, white dwarf.

Late-type Stars

Emission-line Red Dwarfs Stars, dMe

dM- emission often in CaII H & K lines

dMe- emission in Ha

Sample of Ha Emission-line in dMe Stars

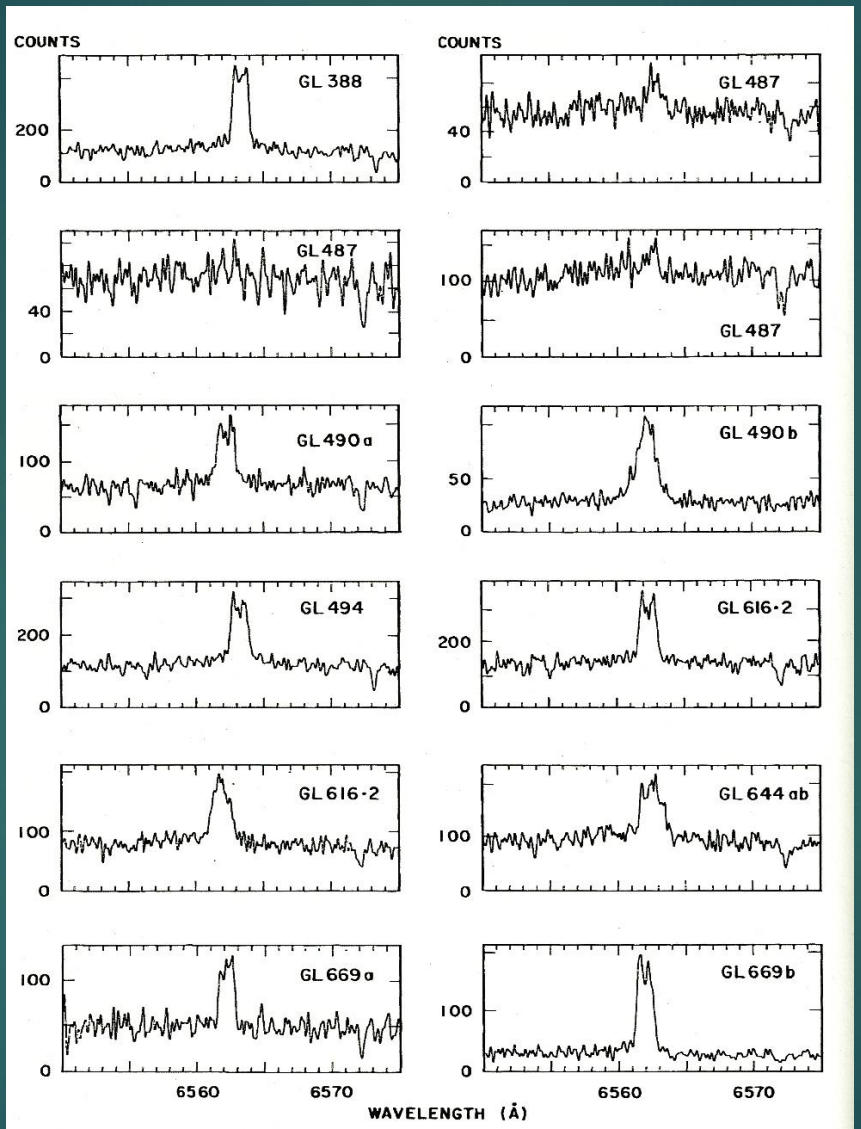

Figure 6.6: Samples of *Hα* emission lines in dMe stars. The stars are mainly designated by Gliese's catalogue number. The same stars in different panels show the spectra taken at different époques. (From Stauffer and Hartmann 1986)

Ha Line Profiles of dM and dMe Stars

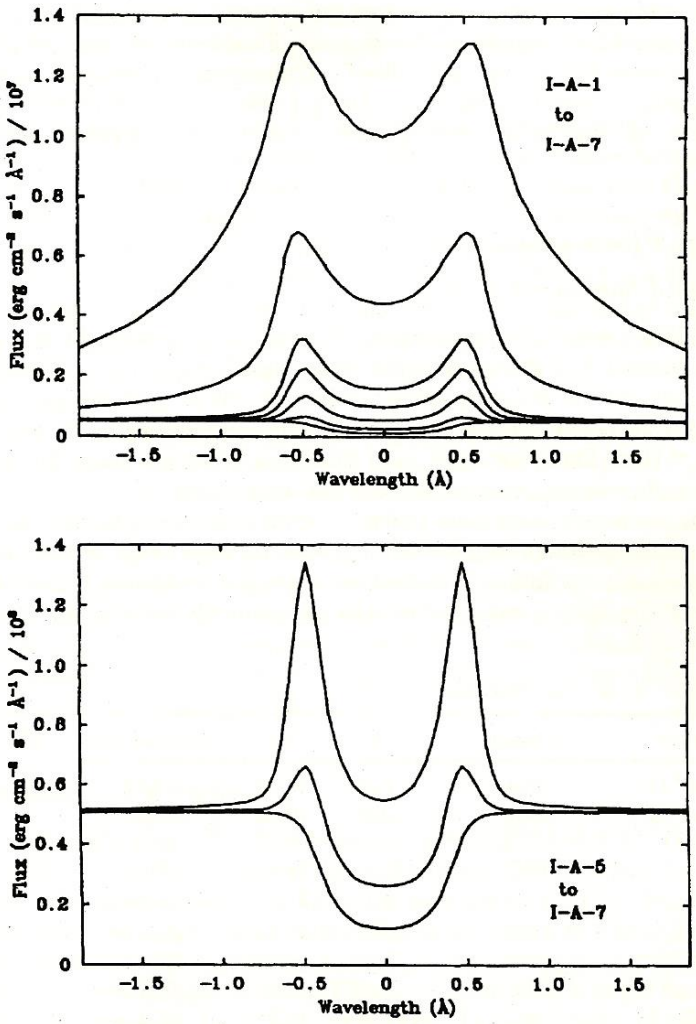

Figure 6.7: *Hα* line profiles in the model calculation for dM and dMe stars. Upper panel indicates the change of profiles caused by the change of column density (from log $(M) \sim -5$ to log $(M) \sim -3$). Lower panel shows the enlarged profile to change from absorption to emission. (From Houdebine et al. 1995)

Flare Stars

There many stars flare up in both light level and spectra

Types:

Fast flare stars, < 30 minutes

Slow flare stars, between 30-40 minutes

Out Burst of Flare Star

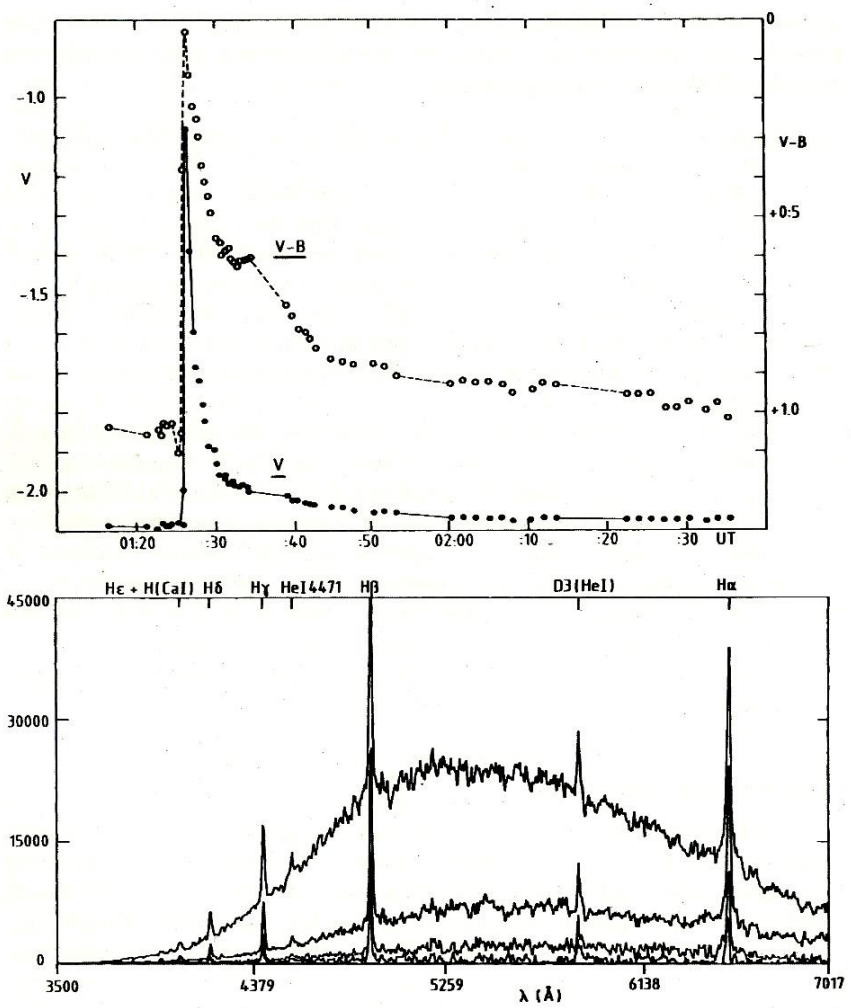

Figure 6.8: Flare burst of UV Ceti on December 23, 1985. Upper panel shows the brightness (modified V band) and (V–B) light curves. Lower panel shows spectra of the flare. The diagram shows successive spectra of the flare component (preflare spectrum subtracted) in declining phase from top to bottom (flare maximum at the top). The times of observations are approximately at 01:26 (at max.), 01:28, 01:29, and 01:30 UT, from top to bottom. (From de Jager et al. 1989)

Emission Flux of Line in Red Giants

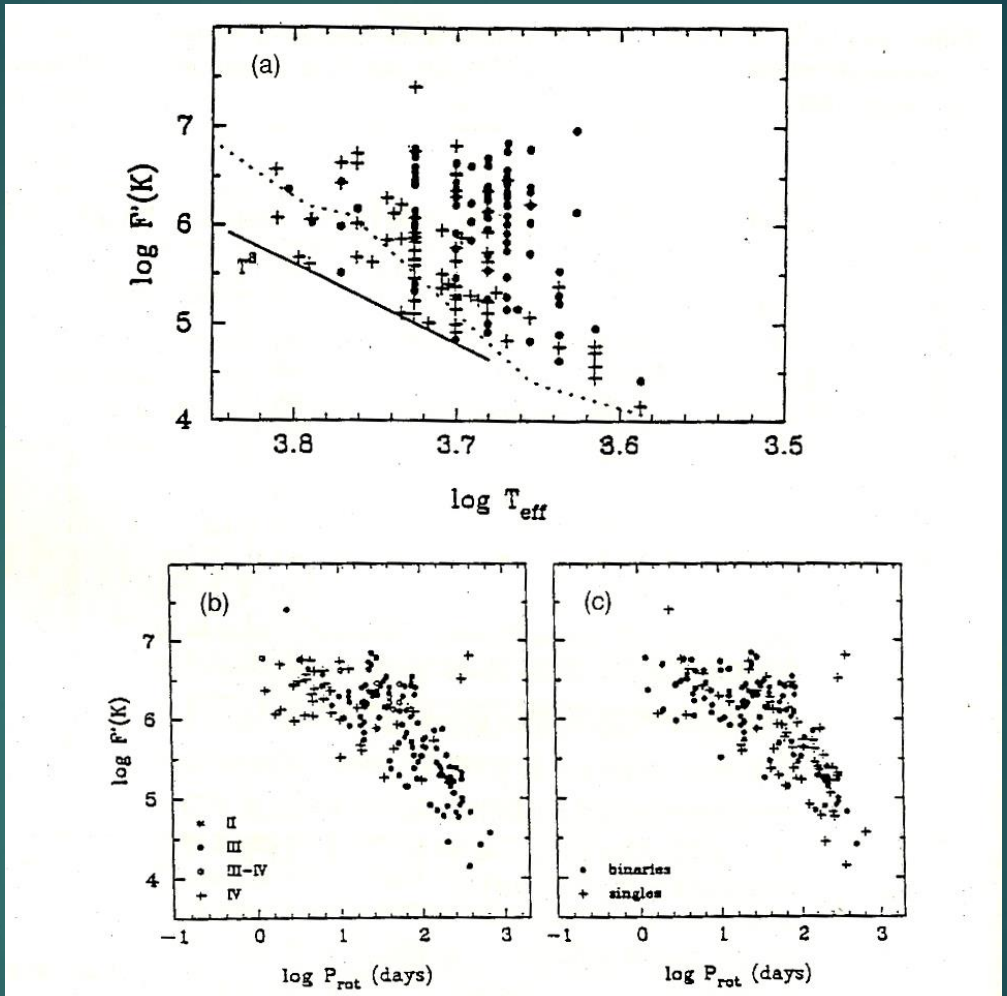

Figure 6.16: A, The emission flux of K line as a function of stellar effective temperature. The dotted lines is the theoretical prediction by the basal atmosphere theory, the full line denotes the empirical lower limit. Panels B and C yield the relation between emission flux of K line and the rotational period, where Panel B distinguish the stellar luminosity, and C the distinction whether singles or binaries. (From Strasmeier et al. 1994)

Phase Change in Balmer Lines in Long Period Variables

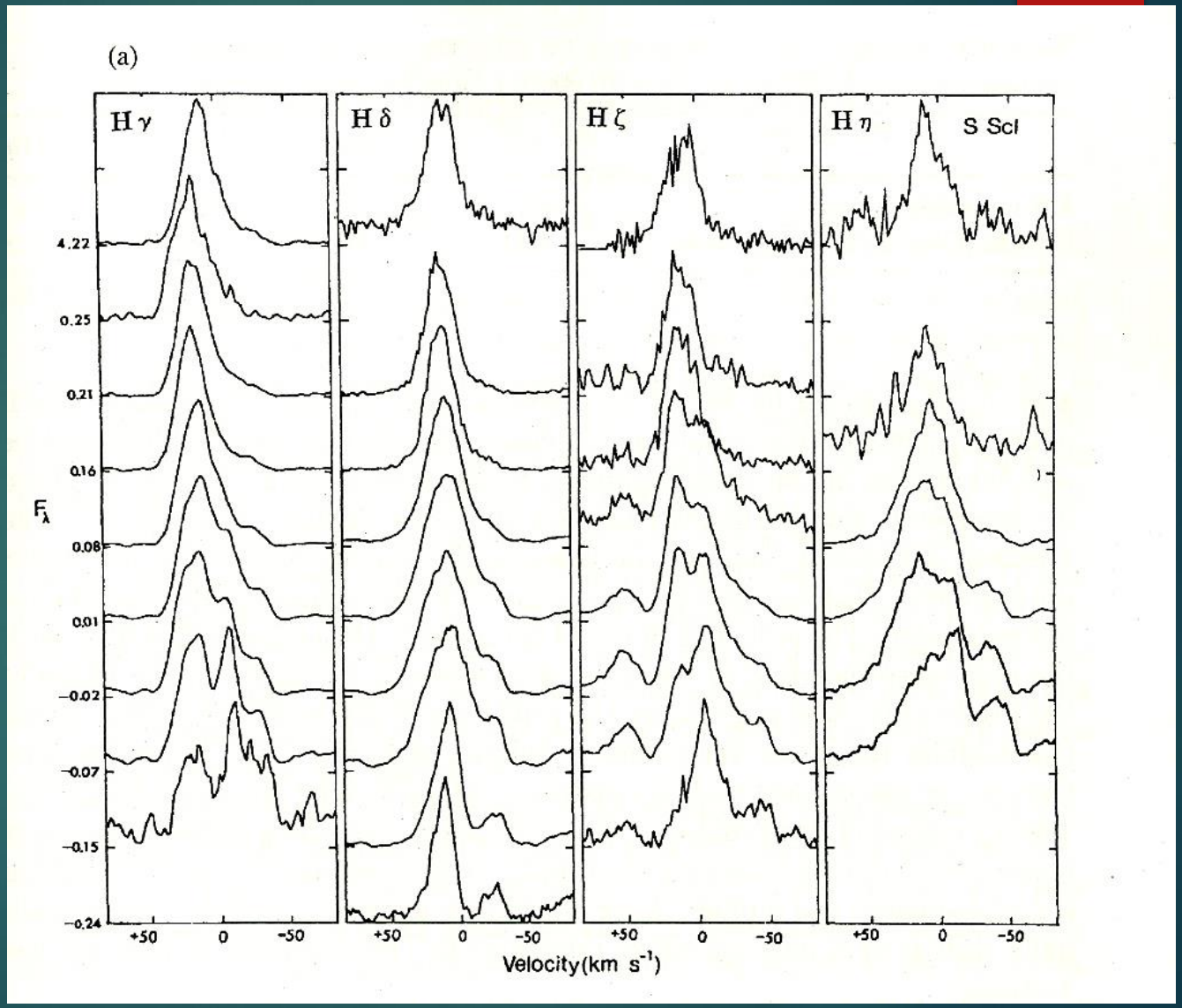

Chromospheric Activities of RS CVn Stars

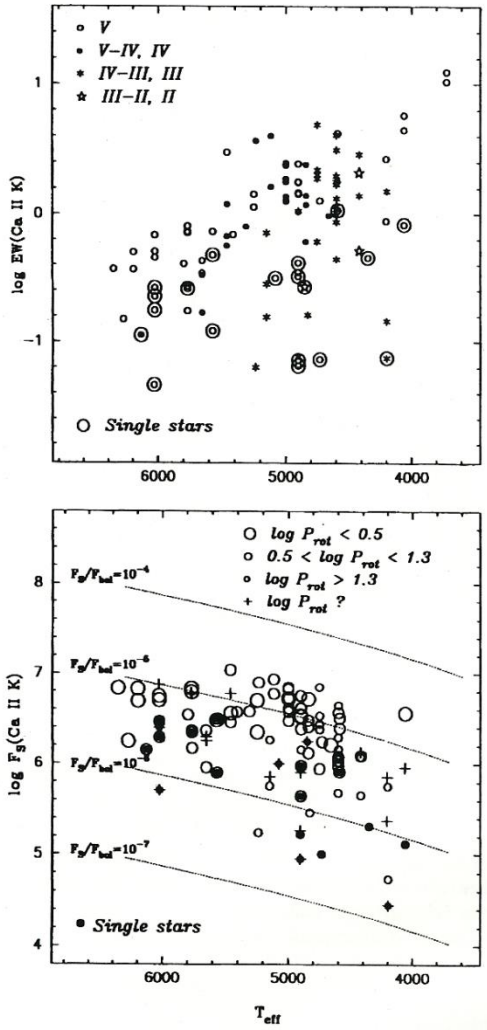

Figure 6.25: Chromospheric activities of RS CVn stars in CaII K line. Excess CaII K emission equivalent width, EW (CAII K) (upper panel), and CaII surface flux, F_S(CaII K) (lower panel). Both panels are plotted against effective temperature. In the upper panel different symbols are used to represent the stars with different luminosity class. In the lower panel the size of the symbols is inversely proportional to the rotation period (P_{rot}). The dashed lines indicate constant F_S (CaII K)/F_{bol} ratios. (From Montes et al. 1996)

Types of RS CVn Stars

Group 1: Both components are dwarf stars (21 systems). When both components have the same or very similar spectral type, the observed emissions are also very similar (YY Gem, BF Lyn, AS Dra, etc.). However, when the components of the system have different spectral types, the hot component tend to be more active (DH Leo, BY Dra, KT Peg, etc.), or even only hot components are active (MS Ser, V815 Her, V775 Her, etc.).

Group 2: Two-subgiant systems (23 systems). In most cases the cool component is responsible for the activity. In 7 systems, CaII H and K emissions are observed from both components, although the cool component tends to be more active in the system (RS CVn, V711 Tau, etc.).

Phase Variation of Ha Profile of RS CVn Stars

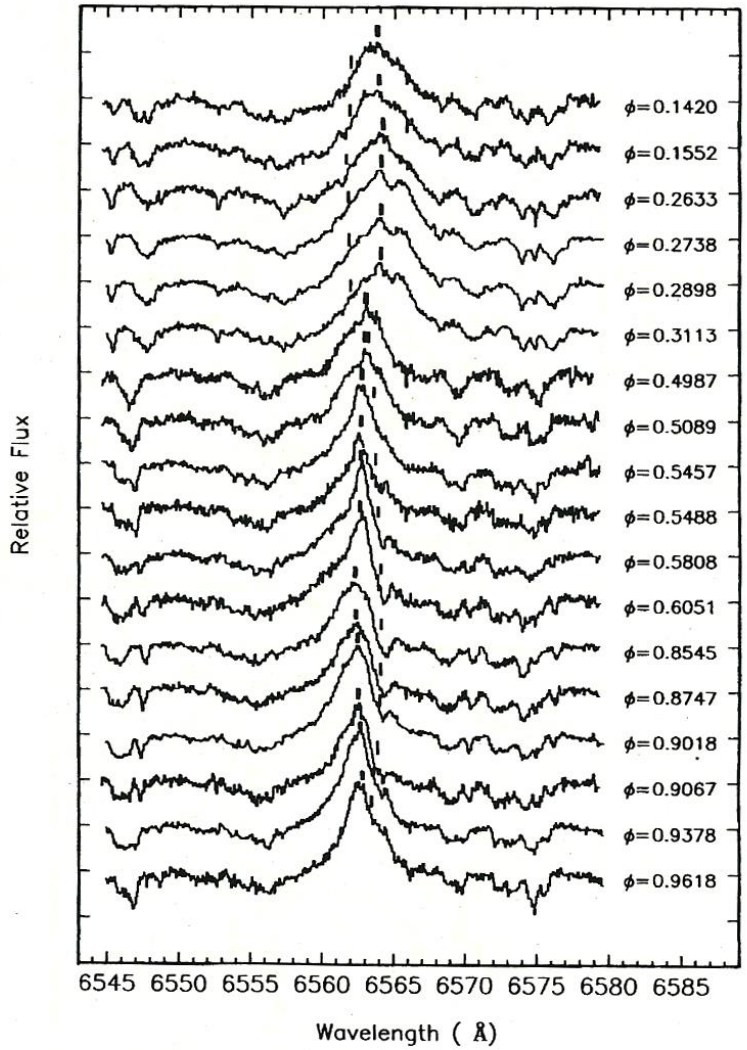

Figure 6.26: Phase variation of the Hα profile of the RS CVn type binary V711 Tau (HR1099). Phase $\varphi = 0$ corresponds to the primary minimum (K1 star is just in front of the secondary G5 star). The solid and thin marks on the spectra indicate the orbital velocities of the primary and secondary, respectively. (From Zhai and Zhang 1996)

Schematic Mass-transfer of RS CVn Stars

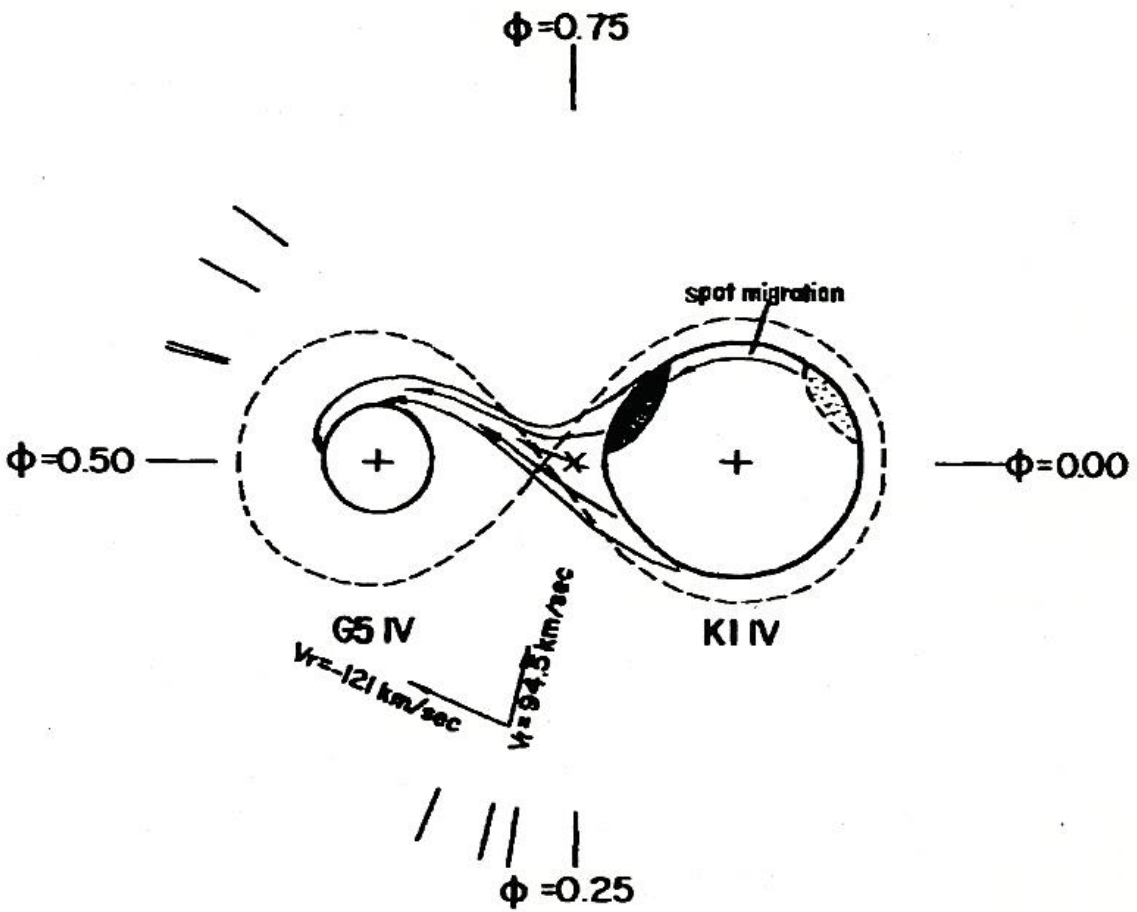

Figure 6.27: A mass-transfer model for the RS CVn type binary V711 Tau (HR 1099). The observed heliocentric radial velocities V1 = 94.5 km s^{-1} at $\varphi = 0.29$ and $V1 = -121$ km s^{-1} at $\varphi = 0.58$ are indicated. A remarkable spot migration from 1992 September to 1993 January is also illustrated in the figure. (From Zhai and Zhang 1996)

Categories of Cataclysmic Variables, CVs

Classical Novae CN

Recurrent Novae RN

Dwarf Novae DN

Nova-live Variables NL

Schematic Picture of CV Stars

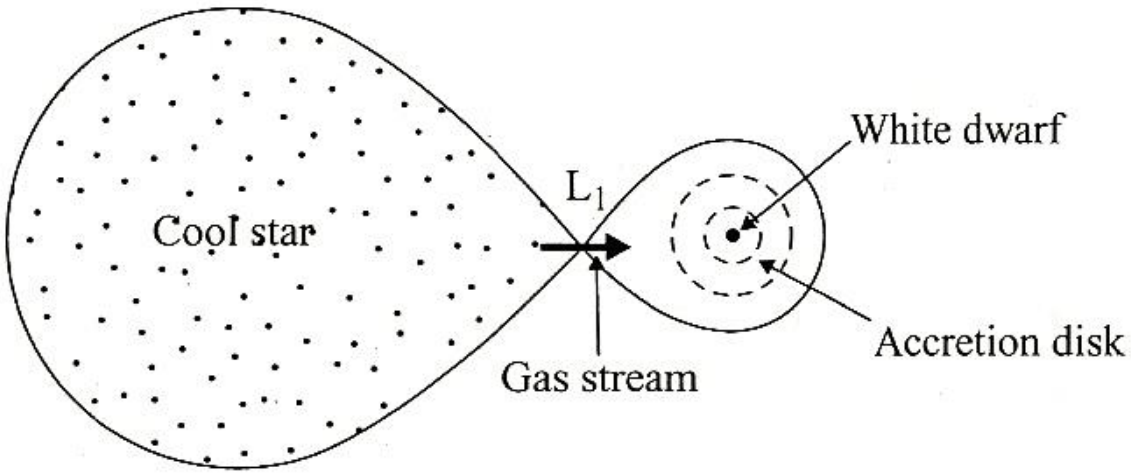

Figure 6.28: Schematic picture of CVs in the orbital plane. Cool star expands to fill the Roche lobe, and a gas stream flows onto the accretion disk of the white dwarf. (From Hoffmeister et al. 1985)

Schematic Diagram of Classical Novae

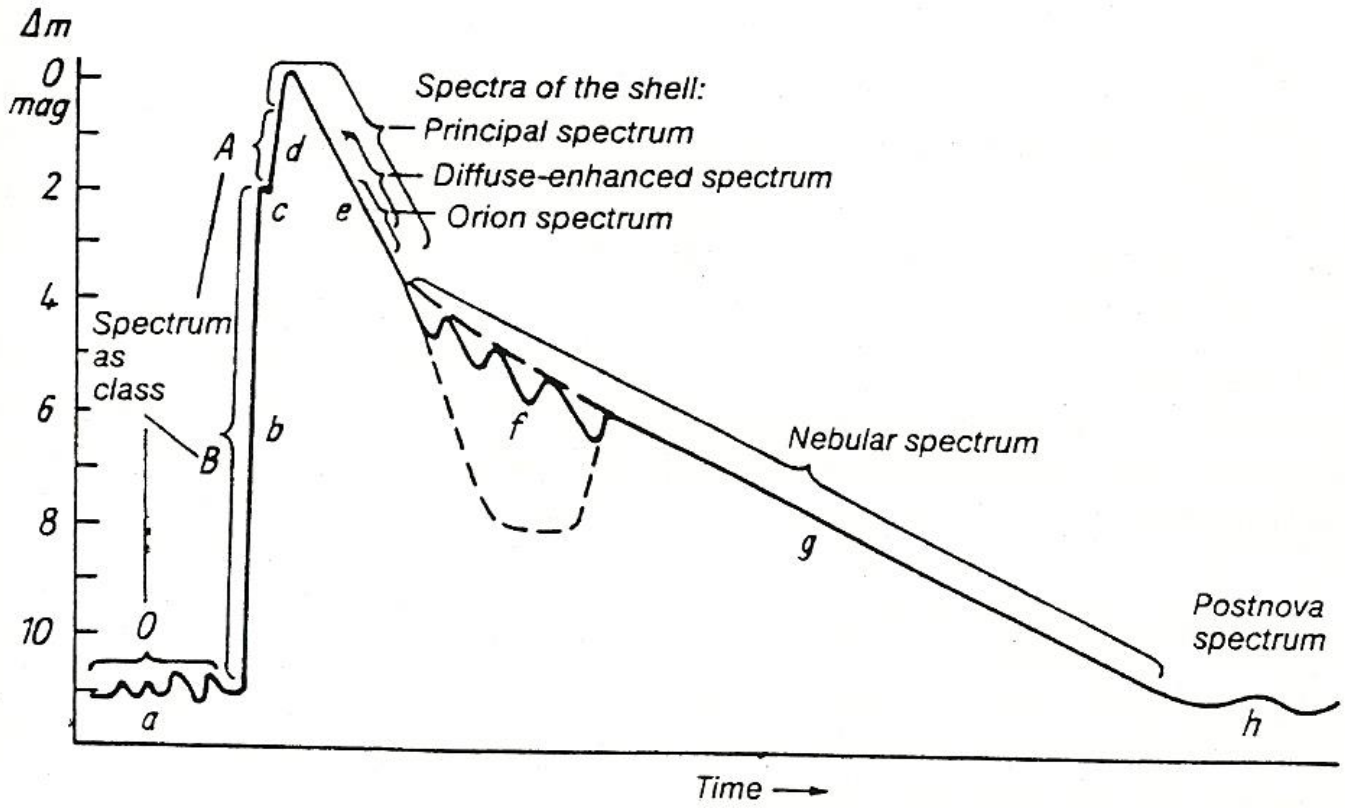

Figure 6.29: Schematic diagram of the luminosity, phase, and spectra for understanding the nomenclature of nova phenomena. The spectral characteristics before and after the maximum phase are also shown. The main signs are mainly based on Hoffmeister et al. (1985) as follows: a, prenova; b, first rise; c, pre-maximum pause; O, B, A prenova to burst spectrum; d, final rise; e, initial decline; f, transition stage; g, final decline; h, postnova. For spectral phase, see text.

Spectral Variation RN Outburst

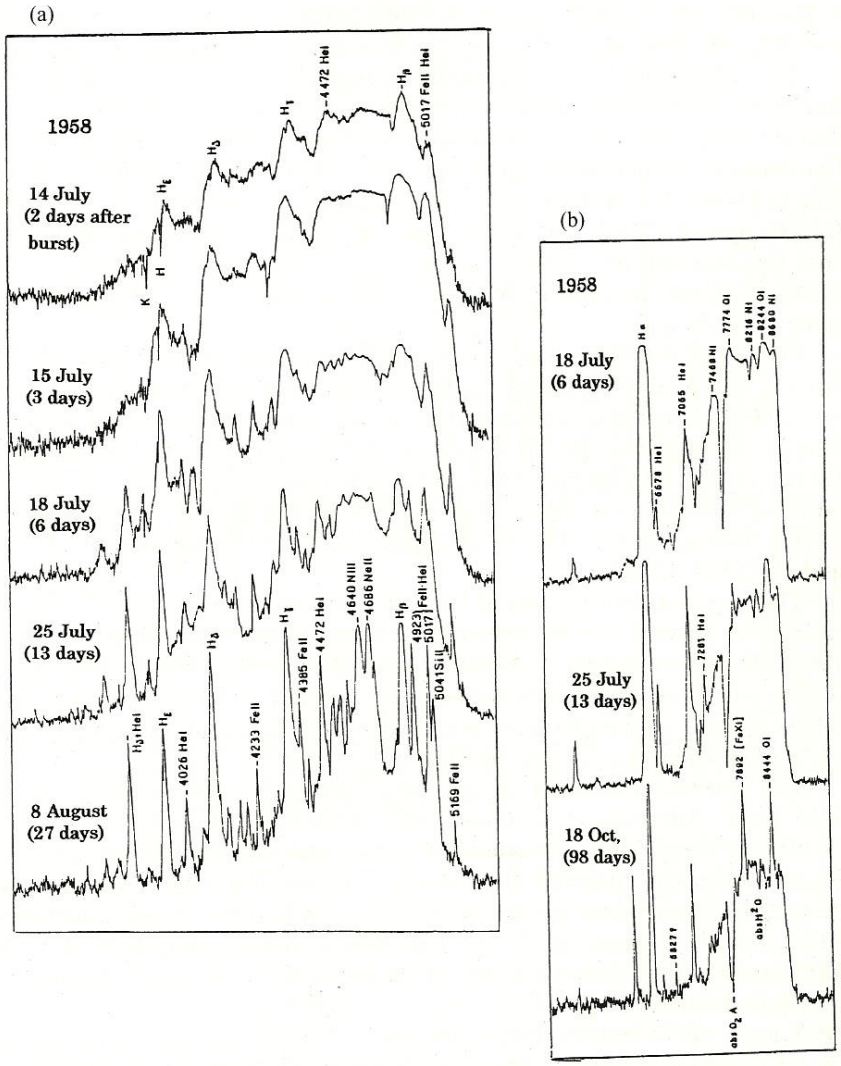

Figure 6.36: Spectral variation of the RN RS Oph in 1958 outburst, observed with 120-cm telescope at Haute-Provence Observatory. Panel (a) denotes the optical-near ultraviolet spectral region and panel (b) the red-near infrared spectral region. (From Dufay et al. 1965)

Types of Dwarf Novae, DN

Types of dwarf novae

Dwarf novae also repeat outbursts like RNe, but with smaller scales as follows:

scale of outbursts—typically 2–5 magnitudes
intervals of outbursts—10 through several 100 days
duration of outburst—around 2 to 20 days

In the quiescent stage, the stars exhibit strong ultraviolet continuum and Balmer emission lines. During the outburst, emission lines are weakened or often disappeared and instead sometimes the He II line appears. A spectral atlas in the wavelength range λ 4000–5000 Å for 48 DNe in outburst state is provided by Morales-Rueda and Marsh (2002).

DNe are classified into the following three subtypes (the number of stars given in bracket for each type is taken from Warner 1995).

U Gem type or SS Cyg type. The interval from burst to burst varies from several days to several years. After an abrupt brightening of 2 to 8 magnitudes, it stays at maximum for 1 to 2 days and declines over several days or weeks (29 stars).

Z Cam type. This type is characterized by the standstill phenomena, i.e., an outburst cycle is interrupted by a phase of more or less constant standstill brightness between the outburst maxima and minima. The duration at standstill varies greatly from star to star, and with different instances of the same star, ranging from a few days up to more than a year (12 stars).

SU UMa type. In this type there are two distinct types of outbursts: normal outburst typically lasting for a few days, and superoutburst occurring after 3 to 10 normal outbursts, and lasting longer with larger amplitudes for about 2 weeks. The orbital periods are very short, mostly within 2 hours (34 stars).

Phase Variation of Ha in Dwarf Nova, DN

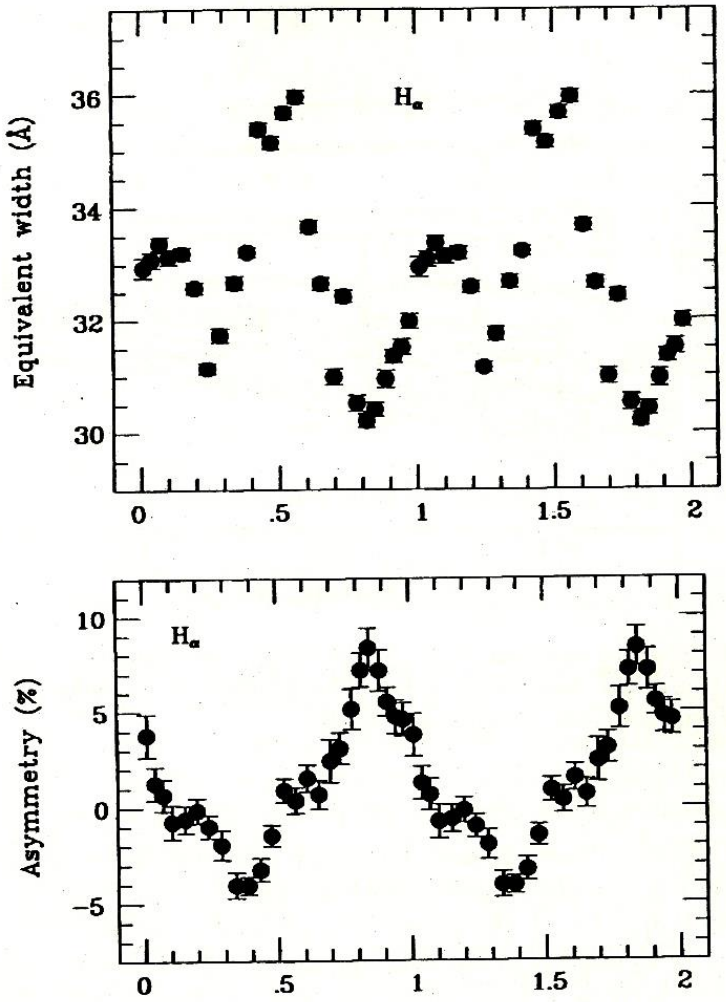

Figure 6.39: Phase variation of the Hα line in the quiescent phase of the dwarf nova SS Cyg. The abscissa is the phase in the orbital period of 6.60 hours. Upper panel: Emission equivalent width in Å. Lower panel: Asymmetry of double peak profile expressed in relative intensities of V (violet) and R (red) components. In the ordinate "plus" denotes V < R and "minus" denotes V > R. (From Martinez-Pais et al. 1994)

Types of Nova-like Variables

Types of nova-like variables

Among the CVs, there are some groups that do not show eruptive phenomena. We call them the nova-like variables (NLs), which are mainly divided into the following two subtypes designated by the appearance of emission spectra.

RW Tri type. Stars reveal almost pure emission spectra with few absorption lines.

UX UMa type. Stars are characterized by pertinent broad absorption with central narrow emission components.

Schematic Geometry of Symbiotic Stars

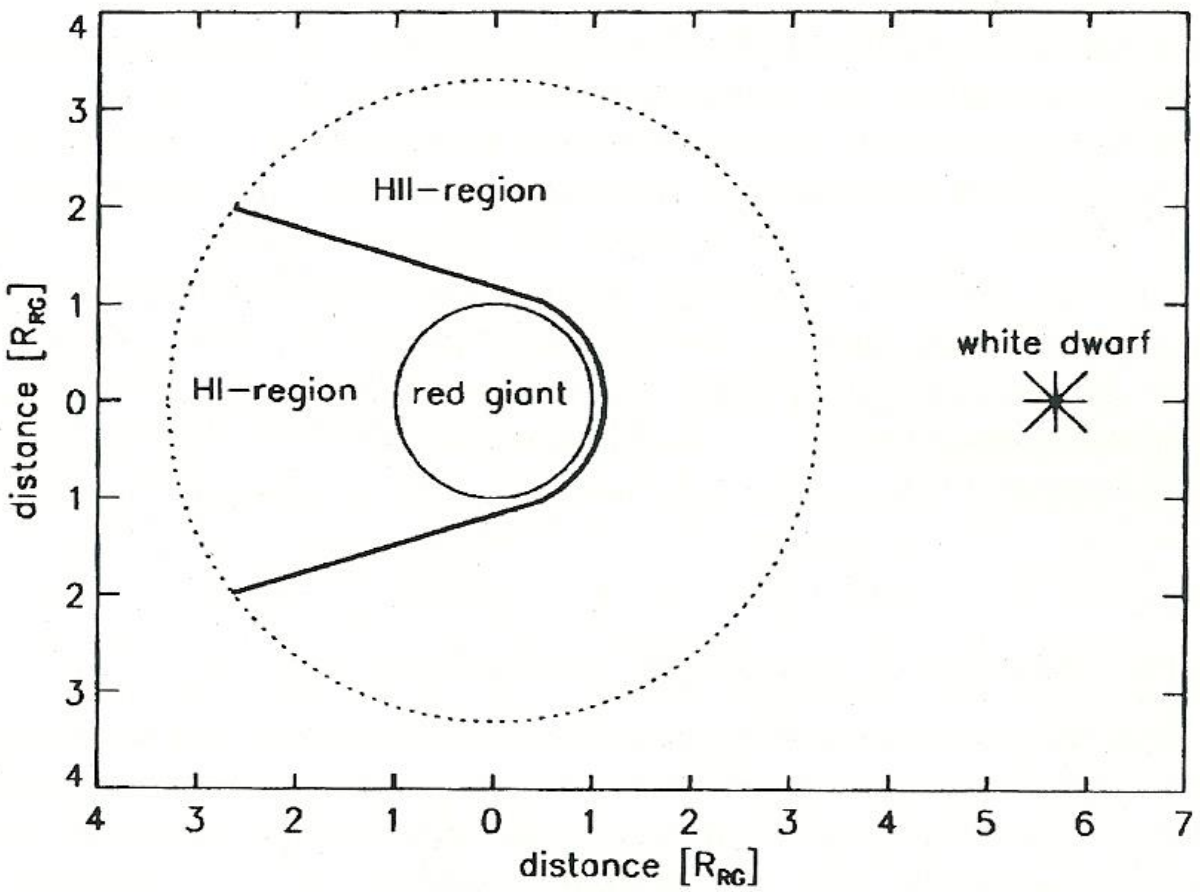

Figure 6.46: Schematic geometry of a Symbiotic star composed of a red giant and a white dwarf. Distance unit is the radius of red giant (R_{RG}). Ionization front separating HI and HII regions in the atmosphere of the red giant is also shown. (From Schwank et al. 1997)

Pre-main Sequence Stars

Hderbig Ae/Be Stars, HES

T Tauri Stars, TTS:
FU Orionis Stars
YY Orionis Stars

List of Herbig Emission-line Stars

Table 7.1: A list of selected Herbig Ae/Be stars

Name	HD/etc	$V^{a}_{\rm mag.}$	Sp. type[b]	IRAS[c]	Nebula[d]	IR-ex.[e]	Hα[f]	X-ray[g]
AB Aur	HD 31293	(6.9–8.4)	B9/A0e+sh	Y	N	I	P	Y
UX Ori	HD 293762	9.2–12.3	A2/3IIIe	Y	N	I	C	—
HK Ori	—	11.63	B8/A4ep	Y	N	I	D	—
T Ori	BD-5^{0}1329	(8.7–12.6)	A3/5eα	N	Y	I	InvP	—
V380 Ori	BD-6^{0}1253	(9.97–10.82)	B8/A1e	Y	Y	I	S	Y
BF Ori	BD-6^{0}1259	(9.60–13.5)	A1/F6e+sh	Y	N	I	D	—
ω Ori	HD 37490	(4.41–4.59)	B3III-IVe	Y	Y	III	D	N
R Mon	BD+8^{0}1427	10.37–11.89	B0e	Y	Y	II	—	—
GU CMa	HD 52721	(6.50–6.72)	B2Vne	Y	—	III	S	N
HR 5999	HD 144668	(6.73–8.47)	A7III-IVe	Y	N	—	D	Y
R CrA	CPD-37^0 8452	10.74–11.50	A5IIe+sh:/F0	Y	Y	II	—	N
MWC1080	—	(11.58–11.67)	B0eq	Y	Y	I	P	Y
V633 Cas	LkHα 198	14.29	B/Ae	Y	Y	II	—	N

[a] $V_{\rm mag.}$: In brackets the magnitudes in other bands such as pg = photographic, B, and R are given. In many case light variations are observed.
[b] Spectral type by different reference is distinguished by slash.
[c] IRAS source: Whether exists or not is shown by Y and N, respectively.
[d] Nebula: The association with nearby nebula is shown by Y or N.
[e] IR excess: The type of excess is shown by Hillenbrand et al. (1992) (see Table 7.2)
[f] Hα emission profile is distinguished as follows (Finkenzeller & Mundt, 1984): S = single peak, D = double peak, P = P Cyg, InvP = inverse P Cyg, C = complex
[g] X-ray source: Whether exists or not is shown by Y and N (Zinnecker and Preibisch 1994).
The third to sixth columns are taken from Thé et al. (1994).

Definition of HES

i) The spectral type is A or earlier, with emission lines
ii) The star lies in an obscured region in HR diagram
iii) The star illuminates fairly bright nebulosity in its immediate vicinity

Difference between HESs and Be stars of same spectral type

a) Infrared excess
b) Time variations
c) Linear polarization
d) Association with star-formation regions

Herbig Ae/Be Stars, HESs

Table 7.1: A list of selected Herbig Ae/Be stars

Name	HD/etc	$V^a_{\rm mag.}$	Sp. type[b]	IRAS[c]	Nebula[d]	IR-ex.[e]	Hα[f]	X-ray[g]
AB Aur	HD 31293	(6.9–8.4)	B9/A0e+sh	Y	N	I	P	Y
UX Ori	HD 293762	9.2–12.3	A2/3IIIe	Y	N	I	C	—
HK Ori	—	11.63	B8/A4ep	Y	N	I	D	—
T Ori	BD-5^{0}1329	(8.7–12.6)	A3/5eα	N	Y	I	InvP	—
V380 Ori	BD-6^{0}1253	(9.97–10.82)	B8/A1e	Y	Y	I	S	Y
BF Ori	BD-6^{0}1259	(9.60–13.5)	A1/F6e+sh	Y	N	I	D	—
ω Ori	HD 37490	(4.41–4.59)	B3III-IVe	Y	Y	III	D	N
R Mon	BD+8^{0}1427	10.37–11.89	B0e	Y	Y	II	—	—
GU CMa	HD 52721	(6.50–6.72)	B2Vne	Y	—	III	S	N
HR 5999	HD 144668	(6.73–8.47)	A7III-IVe	Y	N	—	D	Y
R CrA	CPD-37^0 8452	10.74–11.50	A5IIe+sh:/F0	Y	Y	II	—	N
MWC1080	—	(11.58–11.67)	B0eq	Y	Y	I	P	Y
V633 Cas	LkHα 198	14.29	B/Ae	Y	Y	II	—	N

[a] $V_{\rm mag.}$: In brackets the magnitudes in other bands such as pg = photographic, B, and R are given. In many case light variations are observed.
[b] Spectral type by different reference is distinguished by slash.
[c] IRAS source: Whether exists or not is shown by Y and N, respectively.
[d] Nebula: The association with nearby nebula is shown by Y or N.
[e] IR excess: The type of excess is shown by Hillenbrand et al. (1992) (see Table 7.2)
[f] Hα emission profile is distinguished as follows (Finkenzeller & Mundt, 1984): S = single peak, D = double peak, P = P Cyg, InvP = inverse P Cyg, C = complex
[g] X-ray source: Whether exists or not is shown by Y and N (Zinnecker and Preibisch 1994).
The third to sixth columns are taken from Thé et al. (1994).

Characteristics of T Tauri stars:

a) Association of star-forming regions
b) Location on the HR diagram
c) Spectral characteristics- strong stellar activities forming variable emission lines infer the existence of

END

V/R Variation of Be Stars

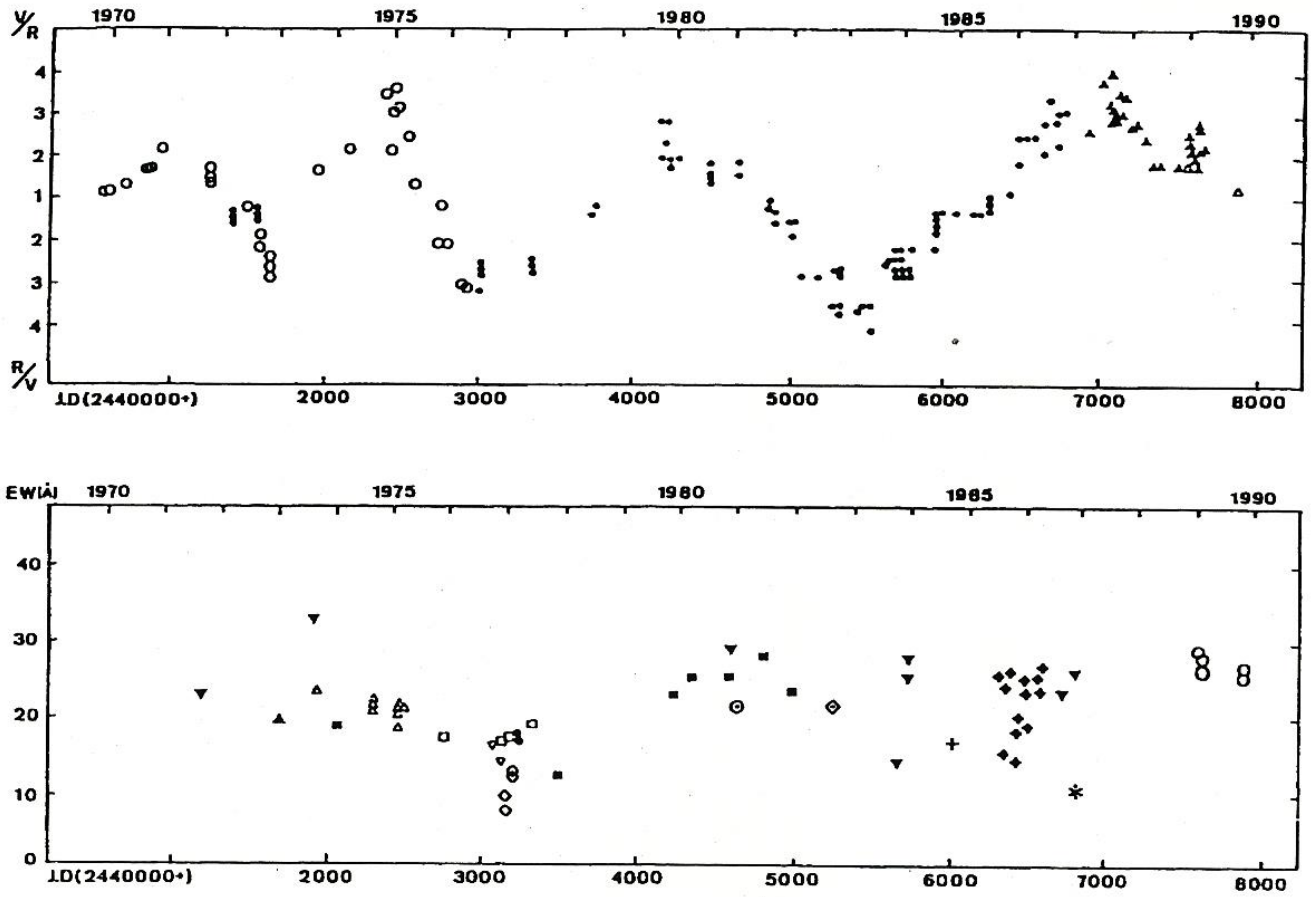

Figure 5.39: Long-term variations in γ Cas observed in the period 1970–1990. The upper panel denotes the V/R (the upper and lower parts of the ordinate give the values of V/R and R/V, respectively) and the lower panel shows the emission-equivalent width of Hα, EW(Å). Different symbols denote the values by different observers. (From Horaguchi et al. 1994)